

Benchmark Generation Framework with Customizable Distortions for Image Classifier Robustness

Soumyendu Sarkar^{†*} Ashwin Ramesh Babu[†] Sajad Mousavi[†] Zachariah Carmichael[†]
Vineet Gundecha Sahand Ghorbanpour Ricardo Luna Gutierrez Antonio Guillen
Avishek Naug
Hewlett Packard Enterprise, USA

{soumyendu.sarkar, ashwin.ramesh-babu, sajad.mousavi, zachariah.carmichael}@hpe.com
{vineet.gundecha, sahand.ghorbanpour, rluna, antonio.guillen, avishek.naug}@hpe.com

Abstract

We present a novel framework for generating adversarial benchmarks to evaluate the robustness of image classification models. Our framework allows users to customize the types of distortions to be optimally applied to images, which helps address the specific distortions relevant to their deployment. The benchmark can generate datasets at various distortion levels to assess the robustness of different image classifiers. Our results show that the adversarial samples generated by our framework with any of the image classification models, like ResNet-50, Inception-V3, and VGG-16, are effective and transferable to other models causing them to fail. These failures happen even when these models are adversarially retrained using state-of-the-art techniques, demonstrating the generalizability of our adversarial samples. We achieve competitive performance in terms of net L_2 distortion compared to state-of-the-art benchmark techniques on CIFAR-10 and ImageNet; however, we demonstrate our framework achieves such results with simple distortions like Gaussian noise without introducing unnatural artifacts or color bleeds. This is made possible by a model-based reinforcement learning (RL) agent and a technique that reduces a deep tree search of the image for model sensitivity to perturbations, to a one-level analysis and action. The flexibility of choosing distortions and setting classification probability thresholds for multiple classes makes our framework suitable for algorithmic audits.

1. Introduction

Neural networks’ susceptibility to adversarial perturbations has raised concerns about their reliability. Adversarial perturbations are slight alterations to input data that can

cause neural networks to make confident yet incorrect predictions. Despite efforts to understand and counter adversarial perturbations, existing defense strategies have shown limited improvements in robust accuracy. This emphasizes the need for alternative approaches to evaluate and enhance neural network robustness. Recent research suggests that generating additional subsets from the main dataset through perturbations/augmentations can improve robustness in fully-supervised and semi-supervised settings [17]. To utilize the original training set more effectively, modifications are introduced. One popular recent approach, proposed by Hendrycks and Dietterich (2018), aims to evaluate model robustness and ultimately enhance it [17].

We propose a machine learning-driven adversarial data generator that introduces natural distortions to create an adversarial subset from an original dataset. Our approach formulates the generation of adversarial samples as a Markov Decision Process (MDP). By dividing the input sample into patches, we aim to identify and add distortions to the most vulnerable areas, leading to misclassification. Our generator utilizes an addition and removal mechanism, mimicking a deep tree search to find vulnerabilities and add noise in the right locations. Additionally, our method allows users to incorporate custom datasets and distortion types for generating adversarial samples.

As part of our work, we provide adversarial subsets derived from CIFAR-10 and ImageNet datasets. We evaluated the performance of adversarially trained models using state-of-the-art techniques from the literature on our dataset. The performance of these models on our dataset is noticeably lower than on the clean dataset and a competitor’s benchmark [17]. We achieved an average L_2 value of 2.48 (evaluated over 1,000 ImageNet samples) and a maximum of 4.74. Our benchmark will assist future initiatives in building robust architectures, which is crucial considering the increasing concerns and requirements for robust deep-

*Corresponding author. †Equal contribution.

learning models.

The main contributions of this paper are as follows:

- We propose a framework to generate adversarial benchmarks with a custom mix of distortions for evaluating the robustness of image classification models against both true negatives and false positives.
- We enable robustness audits for distortions characteristic of use cases at deployment for multiple distortion thresholds.
- We achieve competitive performance with the state-of-the-art on multiple metrics of minimum distortions needed for misclassification.
- We are competitive with the state-of-the-art on improving robustness with adversarial training.

2. Related Works

2.1. Data augmentation and adversarial samples for improving robustness

Several data augmentation techniques have been proposed to enhance the robustness of deep learning models. Cutout [9] masks out regions of input images which forces models to rely on alternative informative features. Mixup [54] generates virtual training samples by interpolating between pairs of images and labels, reducing overfitting and increasing robustness. Manifold Mixup [49] extends this idea by interpolating between feature representations. CutMix [53] combines Cutout and Mixup by replacing masked regions with patches from other images. AugMix [18] applies diverse augmentations to images, encouraging models to learn from a wide range of variations. Randaugment [7] applies random sequences of augmentation policies. RandConv [52] applies random convolutions as data augmentation. ALT [14] uses adversarially learned transformations to obtain both objectives of diversity and hardness at the same time. AutoAugment [6] and other recent works [33–35] use Reinforcement Learning (RL) to discover optimal data augmentation policies. These techniques manipulate training data through various transformations, improving the models’ robustness and generalization to adversarial perturbations. Besides RL has been used to solve various problems successfully [26, 36–42, 44].

2.2. Adversarial training for improved robustness

Recent research has explored various approaches to improve the robustness and out-of-distribution (OOD) performance of deep networks. Diffenderfer et al. [10] focused on compressing deep networks to enhance OOD robustness, demonstrating improved performance in handling OOD samples through network compression techniques. Kireev et al. [20] investigated the effectiveness of

adversarial training against common corruption, identifying strengths and limitations of this approach. They explored the performance of adversarially trained models and suggested areas for improvement. Modas et al. [25] proposed PRIME, a framework that leverages primitive transformations during training to enhance robustness against common corruptions, achieving significant improvements in model performance on corrupted inputs. Wang et al. [50] introduced better diffusion models in adversarial training to enhance its effectiveness against adversarial attacks. Tian et al. [47] conducted a comprehensive analysis of the robustness of Vision Transformers (ViTs) towards common corruptions. Geirhos et al. [12] presented a study on the bias toward texture in ImageNet-trained Convolutional Neural Networks (CNNs), showing their reliance on texture rather than shape cues. Erichson et al. [11] developed NoisyMix, a framework that combines data augmentations, stability training, and noise injections to improve the robustness of deep neural networks.

2.3. Benchmark to evaluate robustness

Data augmentation techniques and benchmark datasets play a crucial role in evaluating and enhancing the robustness of image classification models. Hendrycks and Dietterich [17] introduced multiple datasets based on ImageNet and used as benchmarks for evaluating the robustness of models to input corruptions. **ImageNet-C** contains common visual corruptions applied to the ImageNet dataset and allows researchers to assess model performance under various types of visual distortions. **ImageNet-A** focuses on evaluating robustness to common image corruptions by providing a standardized evaluation environment. **ImageNet-P**, on the other hand, assesses the vulnerability of models to subtle perturbations by introducing imperceptible changes to deceive the models while maintaining visual similarity. The **Adversarial Robustness 101 (AR101)** benchmark [5] provides a comprehensive evaluation of model robustness against different attack types using the CIFAR-10 and CIFAR-100 datasets. PACS, Office-Home, MNIST-C, and WILDS benchmark datasets [1, 24, 27, 32] are designed to evaluate the domain adaptation and out-of-distribution robustness of the models. Lastly, the **Robustness via Dataset Manipulation (RoD)** [43] benchmark focuses on evaluating adversarial robustness against physical-world attacks by including real-world images with physical modifications. These benchmarks enable researchers to compare the performance of models and defense techniques in challenging scenarios.

3. Design of the Benchmark Generator

The evaluation for a machine learning model can be represented as $y = \operatorname{argmax}_f(x; \theta)$, where x denotes the input image, y represents the prediction, θ represents the

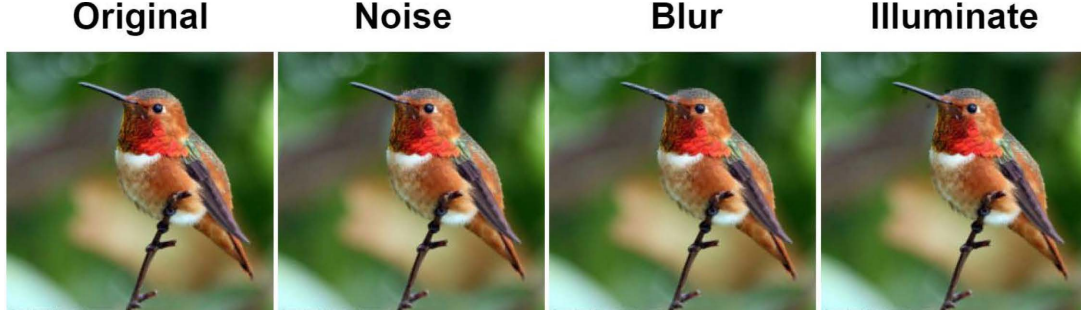


Figure 1. Adversarial samples with multiple distortion types (original picture from ImageNet)

model parameters, and the function f represents the machine learning model’s output,

3.1. Markov Decision Process (MDP) formulation

3.1.1 MDP for un-targeted attack

An un-targeted black-box adversarial sample generator, used for true negative evaluation, without access to the θ , generates a perturbation δ such that $y_{\text{true}} \neq f(x + \delta; \theta)$. L_p norms specify the distance between the original and the adversarial sample, $D(x, x + \delta)$. Our objective is to cause misclassification while keeping D to a minimum.

State S_t contains a number of lists related to the classification probability and sensitivity of the image regions. Action A_t represent the perturbation to obtain the adversarial sample defined as:

$$A_t : x \rightarrow x + \delta_t, \quad (1)$$

where δ_t defines the perturbation at time step t , or more specifically which patches of the original sample x are going to be distorted. We define a probability dilution (PD) metric, which measures the extent to which the classification probability shifts from the ground truth to the other classes. The difference between the PD of the altered and the original image as a result of an action at each step (ΔPD), is a measure of the effectiveness of the action. Moreover, the change in L_2 distance (ΔL_2) as a measure of the distortion added is the cost for action. The reward is defined by the normalized PD as represented in equation 2.

$$R_t = \Delta\text{PD}_{\text{norm}} = -\Delta\text{PD}/\Delta L_2 \quad (2)$$

The change in the distribution of the probabilities across classes is updated in the state vector at every step such that the RL agent can choose the optimum action at every step, maintaining the L_p and the number of steps (queries).

3.1.2 MDP for targeted attack

A targeted black-box attack, used for false positive evaluation, without access to the θ generates a perturbation δ such that $y_{\text{target}} = f(x + \delta; \theta)$ s.t. $y_{\text{target}} \neq y_{\text{true}}$. L_p norms specify

the distance between the original and the adversarial sample, $D(x, x + \delta)$. Our objective is to cause misclassification while keeping D to a minimum. The action A_t will be defined as in equation 1.

We define a probability enhancement (PE) metric, which measures the extent to which the classification probability of the non-ground truth target class goes up. The difference between the PE of the altered image and the original image as a result of an action at each step (ΔPE), is a measure of the effectiveness of the action. Moreover, the change in L_2 distance (ΔL_2) as a measure of the distortion added is the cost for action. The reward is defined by the normalized PE as represented in equation 3.

$$R_t = \Delta\text{PE}_{\text{norm}} = \Delta\text{PE}/\Delta L_2 \quad (3)$$

The change in the distribution of the probabilities across classes is updated in the state vector at every step such that the RL agent can choose the optimum action at every step, maintaining the L_p and the number of step/queries.

3.2. Dual-action speedup for Deep Tree Search

3.2.1 Overview and Modification to MDP

In the proposed method, the input image is divided into square patches of size $n \times n$. For a true negative case, the sensitivity of the ground truth probability (P_{GT}) to addition and removal of distortion is computed for each patch. Based on this sensitivity information, our agent takes two actions at each step: select patches to which distortions are added and selected patches to which distortions are removed. In such a case we can define the state S_t and action A_t for timestep t as:

$$S_t = S_t^+ + S_t^- \quad (4)$$

$$A_t : x \rightarrow x + \delta_t^+ - \delta_t^-, \quad (5)$$

where for timestep t , S_t^+ is the state after the add distortions perturbation δ_t^+ is performed, and S_t^- is the state after the remove distortions perturbation δ_t^- is applied.

This process is iteratively performed until the model misclassifies an image or until the budget for the number of maximum allowed steps is reached. In the case of mixed

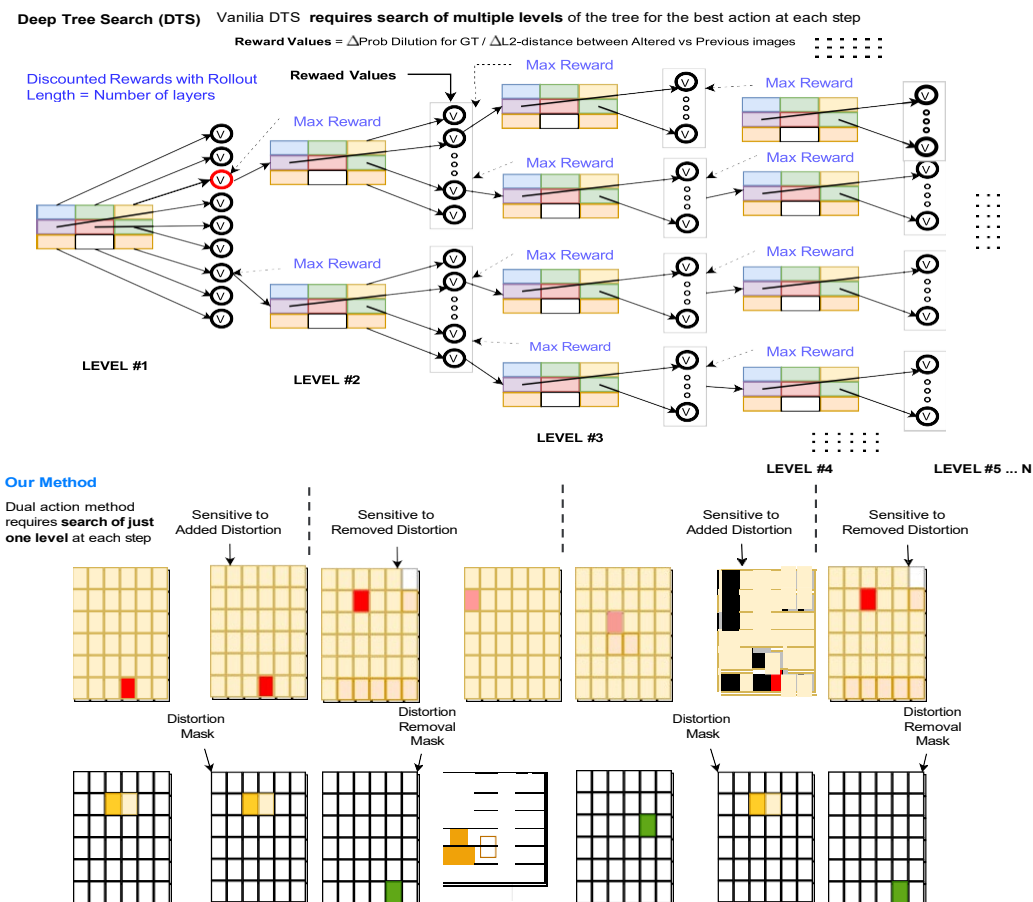


Figure 2. Dual-action architecture simplifying deep tree search

filter setting, the RL agent also needs to choose the optimal type of distortion filter for each step. For introducing the distortion at different threshold levels for untargeted adversarial samples, the process continues until the threshold level of distortion is reached.

A similar technique is adopted for false positive benchmark generation with targeted adversarial samples, where the distortions are added to improve the classification probability of a non-ground truth class.

3.2.2 Intuition for dual-action

The idea of having two actions, addition and removal, is inspired by the limitations of the RL techniques used in board games. In that setting, the most effective moves are determined through a computationally expensive process called Deep Tree Search (DTS), which looks ahead multiple layers on a longer time horizon as the game progresses. However, unlike board games, in this problem, we have the ability to undo previous moves if we realize they were suboptimal. In our framework, this is achieved by removing distortions added to patches in earlier steps and adding distortions to

other patches, considering the current state of the modified image. This is similar to replaying all the moves in one step while analyzing the sensitivity of the image only at its current state, without performing a complete tree search.

By adopting this approach, we can significantly reduce the computational complexity from $O(N^d)$ to $O(N)$. Here, N represents the computation complexity of evaluating one level and corresponds to the image size, while d represents the depth of the tree search, which indicates how far ahead we look in the decision-making process.

3.2.3 Sensitivity Analysis

For the sensitivity analysis, distortion filters (masks) of size $n \times n$ are created with specific hyperparameters like distortion levels. These hyperparameters remain constant throughout the experiment. The filters are applied to square patches during training and validation to measure the change in the ground truth classification probability (P_{GT}). The hyperparameters of the distortion filters are chosen with minimal values to gradually introduce distortion and control the L_p norm effectively. The distorted samples are con-

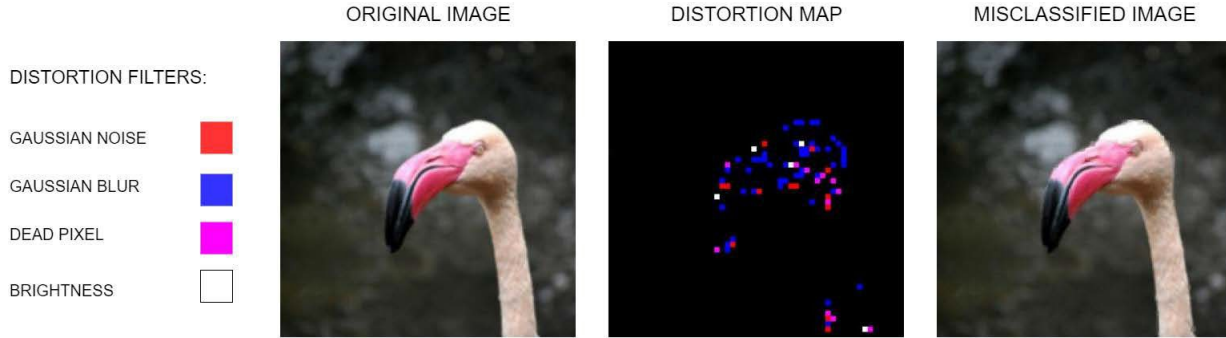


Figure 3. Mix of distortions for Adversarial Sample Generation

strained to the range of $[0, 1]^d$, where d is the dimensionality of the data. When multiple filters are available for the reinforcement learning (RL) agent to choose from, the hyperparameters are selected to have the same impact on the L_p norm after applying any filter.

3.2.4 State Vector

The state vector was designed with the output of the image sensitivity analysis ordered based on the drift in P_{GT} for patches during addition ($LIST^+$) and removal ($LIST^-$) of distortions. In addition, the classification probabilities of each class at every step ($LIST^p$) and the L_p norm are included in the state vector.

3.3. Flexibility to use custom distortions

Our framework offers great versatility by allowing users to apply any type of distortion of their choice. The RL algorithm within the framework learns a policy that can adapt to different filters, ensuring that adversarial samples are generated with minimal distortion, denoted as D . Additionally, the algorithm can handle a combination of filters. At each step, the agent determines which filter (e.g., Gaussian noise, Gaussian blur, brightness adjustment) to use and the number of patches to which the filter should be applied. In our experiments, we explored multiple filters and presented four naturally occurring distortion filters in this paper. Figure 1 displays adversarial examples generated using different filters, while Figure 3 showcases adversarial examples generated with a mixture of various distortion filters.

4. Metrics and Experiments

We evaluate our proposed method with two different types of distortions: Gaussian noise and Gaussian blur. Since these types of common corruptions can be subtle or destructive, we generate data with five levels of severity s and aggregate their scores. Clean error (E^{clean}) is defined as the top-1 misclassification of samples from the clean test set by evaluating the pre-existing classifier on the

un-perturbed dataset. Corrupt error (E^{corrupt}) is defined as the top-1 misclassification of the samples from the corrupt dataset by evaluating the pre-existing classifier on the perturbed dataset. The performance of the classifier across the different severities level of corruption can be represented as:

$$CE^{\text{corrupt}} = \sum_{s=1}^5 E_s^{\text{corrupt}} \quad (6)$$

$$\text{Accuracy}^{\text{corrupt}} = 1 - CE^{\text{corrupt}} \quad (7)$$

$$CE^{\text{degradation}} = \sum_{s=1}^5 (E_s^{\text{clean}} - E_s^{\text{corrupt}}) \quad (8)$$

Furthermore, different corruptions pose different levels of difficulty as the effect of adding Gaussian noise, Gaussian blur, and illumination do not have the same impact on the sample. Note that in our results, for better robustness, we calculate the mean across the different corruption techniques used in this work (denoted as m_{CE}). Finally, accuracy degradation is the decline in the classifier performance when evaluated on the both clean and corrupted dataset.

Our benchmark is used to evaluate models from RobustBench [4], which is a reputable and continuously updated resource that both tracks and benchmarks adversarial robustness methods. The state-of-the-art models are selected by evaluating methods among thousands of papers on difficult benchmarks: L_2 -constrained attacks, L_∞ -constrained attacks, and corruptions on standard image classification datasets. As RobustBench has built its reputation as a core scientific resource for tracking robustness progress, we treat the best-performing methods as the state-of-the-art in the literature. This is further substantiated as methods are included selectively: they cannot generally have non-zero gradients with respect to the input, have a fully deterministic forward pass, nor lack an optimization loop. It is known that the violation of these guidelines does not substantially improve robustness in general [2, 3].

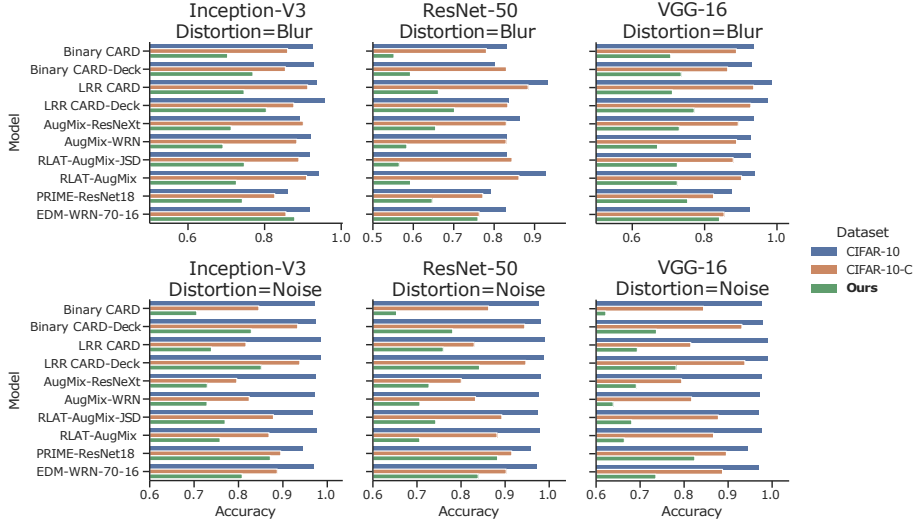


Figure 4. Evaluation of state-of-the-art robustness methods on corrupted versions of CIFAR-10: our corruptions with three victim models (ResNet-50, Inception-V3, and VGG-16) and CIFAR-10-C. Across two kinds of distortions, Gaussian noise and blur, our corrupted version of CIFAR-10 reduces accuracy more than CIFAR-10-C in most cases. Lower accuracy means better performance.

4.1. Compute Details

The computation for the complete pipeline is GPU-dependent and is efficiently batched and scaled on GPUs. Caching techniques were used for pre-computed information such as the noise masks for improved efficiency. Apollo servers with 8 V100 32GB GPUs were used for training and validation, as well as the evaluation of robustness methods. We processed $16 \text{ (images per GPU)} \times 8 \text{ (GPUs)} = 128$ images in a batch for the complete pipeline. See the supplemental material for additional details.

5. Results and Discussion

5.1. CIFAR-10

To validate the effectiveness of our generated benchmark, we compare the performance of state-of-the-art robustness methods between our distorted version of CIFAR-10 [23] and CIFAR-10-C [17]. CIFAR-10-C comprises distorted versions of the CIFAR-10 test set that are applied at five different severity levels. For a fair comparison, we compute the average L_2 distance between the original test set and the CIFAR-10-C test set for each type of distortion. We then employ our framework to generate distorted versions of those data splits for the approximate average L_2 of each CIFAR-10-C severity. Due to our sample generation procedure, we do not set a target L_2 (nor do the generators of CIFAR-10-C) so we must approximate the target average L_2 . In experiments, we set generation parameters empirically and keep splits that have an average L_2 of within 25%. Often, especially with Gaussian blur, our average L_2 is far lower than that of CIFAR-10-C. See Appendix G for further details.

We select the top-10 ranked robustness methods, which includes state-of-the-art diffusion models, on CIFAR-10-C that are reported on the RobustBench benchmark [4] for evaluation: Binary CARD(-Deck) [10], LRR CARD(-Deck) [10], AugMix-ResNeXt [18], AugMix-WRN [18], RLAT-AugMix(-JSD) [20], PRIME-ResNet18 [25], and EDM-WRN-70-16 [50]. For each severity and victim model, we generate two sets of samples with Gaussian noise and Gaussian blur distortions, respectively. We consider VGG-16, Inception-V3, and ResNet-50 as the victim models in experiments. As discussed in Section 3, our framework does not generate a sample if the victim model misclassifies it initially. Hence, we generate distorted samples on a subset of the test set. For a fair comparison, we take the same subset from both CIFAR-10 and CIFAR-10-C to compute clean and corrupted performance, respectively. This sample-wise comparison ensures that harder samples are not excluded or easier samples are not included by one split or another. This is done by storing the indices of every sample in each split, including the original split, CIFAR-10-C split, and our split to prevent samples from inflating or deflating accuracy between splits. The results of these evaluations are shown in Figure 4. For each victim model and distortion, the scores on each CIFAR-10 test set are aggregated across all five levels of severity. For the blur distortion, we cause greater or equal degradation in performance than CIFAR-10-C across all robustness methods and victim models. The exception lies with EDM-WRN-70-16 on samples generated with the Inception-V3 victim model, albeit marginally. Typically, the degradation value is much higher on ours and, sometimes, over double than that of CIFAR-10-C. For the noise distortion, we cause greater or

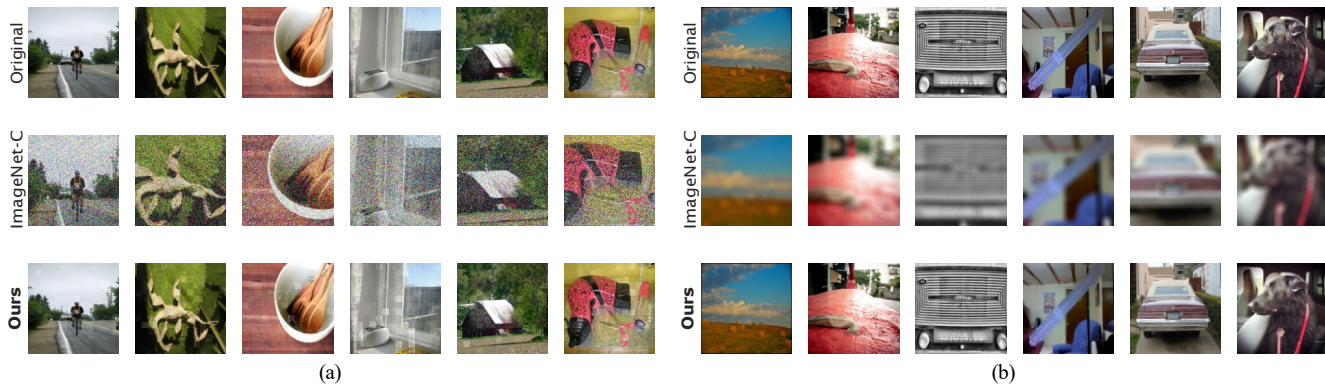


Figure 5. A subset of images from each of original ImageNet, ImageNet-C, and our distorted version of ImageNet. The images shown are for severity level 5 of the Gaussian (a) noise and (b) blur distortions. For the same severity level, images from ours retain much more clarity while being more challenging to classify.

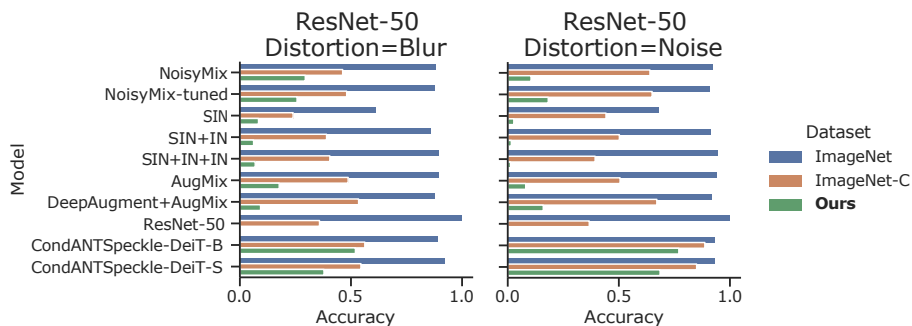


Figure 6. Evaluation of state-of-the-art robustness methods on corrupted versions of ImageNet: our corruptions and ImageNet-C. Our corrupted version of ImageNet reduces accuracy more than ImageNet-C in most cases. Lower accuracy means better performance.

equal degradation in performance than CIFAR-10-C across robustness methods and each victim model. We report the accuracy of the state-of-the-art robustness methods across five severity levels for the Gaussian noise and blur distortions in Appendix A – the accuracy degradation is proportional to the severity level.

5.2. ImageNet

To validate the effectiveness of our generated benchmark, we also compare the performance of state-of-the-art robustness methods between our distorted version of ImageNet and ImageNet-C. Figures 5a and 5b show some examples of the images in original ImageNet, ImageNet-C, and our distorted version of ImageNet. The images shown are for severity level 5 of the Gaussian noise and blur distortions, respectively. Note that ImageNet-C comes center-cropped and thus the full images are not shown. The evaluation here is conducted in the same manner as with CIFAR-10, ensuring that noise levels are similar and that a sample-wise comparison is conducted properly. We select the top-10 ranked robustness methods, which includes state-of-the-art ViTs, on ImageNet-C that are reported on the RobustBench benchmark for evaluation: DeepAugment+AugMix [16], CondANTSpeckle-DeiT-{S,B} [47],

SIN(+IN(+IN)) [12], AugMix [18], standard ResNet-50, and NoisyMix(-tuned) [11].

The results of these evaluations are shown in Figure 6. Similar to our results on CIFAR-10, our distorted version of ImageNet results in greater accuracy degradation across the robustness methods than that of ImageNet-C. Notably, the mean L_2 level of ImageNet-C (99.3) is **69.0% higher than the mean L_2 level on our distorted version of ImageNet (58.8)** for Gaussian noise for the severity level of 5. Furthermore, the mean L_2 level of ImageNet-C (79.8) is *over 3× higher than the mean L_2 level on our distorted version of ImageNet (25.6)* for Gaussian blur. In both cases, we cause *greater accuracy degradation across all robustness models*. We report the accuracy of the state-of-the-art robustness method across five severity levels for the gaussian noise and blur distortions in Appendix A - the accuracy degradation is proportional to the severity level.

5.3. Results on Adversarial Retraining

Table 1 shows retrained robustness of the target model with our framework when compared to retraining with the other competitor approaches. The table presents the degradation error percentages for image classification architectures on the CIFAR-10-C dataset, comparing state-

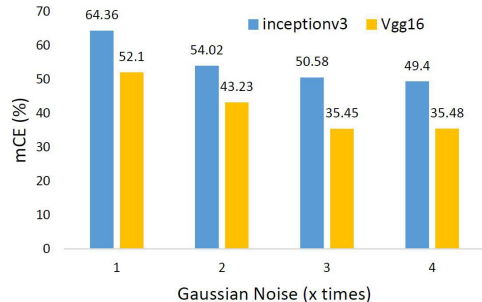


Figure 7. Evaluation of transferability of adversarial samples across other models

of-the-art techniques. The degradation errors for each technique are provided for three different models: ResNet-50, DenseNet, and Inception-V3.

The results show that our framework outperforms the other techniques across all three models. For ResNet-50, we achieved a significantly lower degradation error of 6.0%, compared to Mixup (29.0%), CutMix (31.5%), and AugMix (13%). Similarly, for DenseNet and Inception-V3, our framework also demonstrates superior performance, with degradation errors of 11% and 9.5%, respectively, compared to the other techniques. These findings suggest that our framework effectively has the lowest degradation errors in image classification tasks on the CIFAR-10-C dataset, surpassing the performance of other state-of-the-art techniques like Mixup, CutMix, and AugMix.

Table 1. Degradation error % for image classification architectures on CIFAR-10-C for state-of-the-art techniques. For fairness, all of the techniques were evaluated with the same seed.

Model	Mixup	CutMix	AugMix	Ours
ResNet-50	29.0	31.5	13	6.0
DenseNet	24.0	33.5	15	11
Inception-V3	29	23	11.5	9.5
Mean	27.3	29.3	13.1	8.83

5.4. Transferability across different models

Table 2 represents the ability to transfer the adversarial samples across other primitive models. The adversarial samples are generated to deceive the pre-trained model shown in each row and are tested on the model shown in each column.

From the table, it can be understood that adversarial samples that were generated and evaluated on the same models have 0 accuracy. Furthermore, these adversarial samples still have a significant impact on the other primitive models showing the ability of the proposed method to generalize well. The values are averaged across both Gaussian

blur and Gaussian noise types of distortions. Figure 7 illustrates the transferability of samples generated using the ResNet-50 model with the ImageNet dataset. These samples were tested on Inception-V3 and Vgg16 models under various noise levels. It can be observed that the samples generated by ResNet-50 still exhibit substantial correlation errors across different models. Also, as the noise level increases, the performance tends to decrease.

Table 2. Transferability of adversarial samples generated from CIFAR-10 across other primitive models. The values represent the classification accuracy mCE.

		ResNet-50	Inception-V3	VGG-16
Victim	ResNet-50	0	12.19	8.93
	Inception-V3	20.17	0	12.16
	VGG-16	16.90	16.70	0

6. Limitations

The proposed method focuses on vulnerabilities of image classifiers from distortions present at deployment by providing the customization option. Our results with CIFAR-10-C benchmark show that our method is more effective in identifying vulnerabilities with optimal distortions which are generalizable across models. The nature of the distortion filters used by our model uncovers the broad vulnerabilities of the deployed model, but does not enable unnatural artifacts.

7. Conclusion and Future Work

This paper presents a novel approach to address the challenge of evaluating and improving the robustness of neural networks against adversarial perturbations. The proposed ML-driven adversarial data generator introduces naturally occurring distortions to the original dataset, creating an adversarial subset. By formulating the problem as an MDP, the generator effectively identifies and adds distortions to the most vulnerable areas of the input. This approach demonstrates competitive performance with state-of-the-art techniques, providing a benchmark for evaluating the robustness of image classification models. Additionally, the framework allows for the inclusion of custom distortion types, adversarial thresholds, and datasets, enabling tailored evaluations and audits for specific use cases. The results highlight the importance of building robust deep-learning models and offer valuable insights for future research and development in this area. Overall, this work contributes to the advancement of reliable and resilient deep learning architectures through the generation of adversarial benchmarks and the exploration of improved adversarial training methods. In the future, we will include evaluations on additional naturally occurring perturbations.

Supplemental Section

A. Additional ImageNet Results

We report the accuracy of state-of-the-art **RobustBench** [4] robustness methods across five severity levels for the Gaussian noise and blur distortions in Figure 8. The robustness methods perform worse on our split. The accuracy degradation is proportional to the severity level. Notably, the mean L_2 level of ImageNet-C (99.3) is **69.0% higher than the mean L_2 level on our distorted version of ImageNet** (58.8) for Gaussian noise for the intensity level of 5. Furthermore, the mean L_2 level of ImageNet-C (79.8) is **over 3× higher than the mean L_2 level on our distorted version of ImageNet** (25.6) for Gaussian blur. In both cases, we cause **greater accuracy degradation across all robustness models**.

A.1. Evaluating on different filters

Patch Size	AVG.Q	Max. L_2 (avg.)	ASR %
Gaussian Noise	166	4.74(2.48)	100
Illumination	266	6.94(3.93)	100
Gaussian Blur	201	9.3(5.33)	100
Dead Pixel	75	21.16(13.58)	100

Table 3. Comparison of maximum L_2 , average queries and Average Success rate with different **distortion filters with RLAB**. (avg) represents average L_2 over all samples **Dataset:** ImageNet, **Model:** ResNet-50

Table 3 represents the performance of the proposed approach with different filters. From the table, it can be observed that the approach generates the best results for Gaussian noise followed by the illumination filter for the ImageNet dataset. For brightness, the best results were obtained for the brightness value of -0.1 with values ranging between (-1, 1). For DeadPixel, the percentage of pixels to be dropped for a given patch was set to 50 percent. For Gaussian blur, the standard deviation was set to 1. The standard deviation controls the amount of blurring with a larger value (> 1) creating significantly higher blurring compared to a smaller value. The performance of the Gaussian noise better than the other filters could be due to the strong nature of noise-based distortion proved in numerous works [28, 31].

B. Additional CIFAR-10 Results

We report the accuracy of state-of-the-art **RobustBench** [4] robustness methods across all severity levels for the Gaussian noise distortion in Figure 9. Across the Inception-V3 and ResNet-50 victim models, robustness methods perform worse on our split on average. The ac-

curacy degradation is proportional to the severity level. As explained in the main text, the samples generated with the VGG-16 victim model did not transfer for the Gaussian noise distortion.

C. Error Bars

Here, we reported error bars for applicable experiments. For the robustness experiments comparing with CIFAR-10-C and ImageNet-C, the robustness models from RobustBench have a single set of weights provided, evaluations on CIFAR-10-C and ImageNet-C are deterministic (the splits are fixed), and evaluations on our distorted versions of CIFAR-10 and ImageNet are deterministic (the splits are fixed). Thus, *there are no error bars to report*. For the re-training,

D. RobustBench and the State-of-the-Art in Adversarial Robustness

RobustBench [4] is a reputable and continuously updated resource that both tracks and benchmarks adversarial robustness methods. The state-of-the-art is selected by evaluating methods among thousands of papers on difficult benchmarks: L_2 -constrained attacks, L_∞ -constrained attacks, and corruptions on standard image classification datasets. As RobustBench has built its reputation as the core scientific resource for tracking robustness progress, we treat the best-performing methods as the state-of-the-art in the literature. This is further substantiated as methods are included selectively: they cannot generally have non-zero gradients with respect to the input, have a fully deterministic forward pass, nor lack an optimization loop. It is known that the violation of these guidelines does not substantially improve robustness in general [2, 3]. In our experiments, our distorted version of ImageNet and CIFAR-10 cause further degradation on these state-of-the-art methods than the challenging benchmarks evaluated within RobustBench. This degradation also is realized with less distortion (lower L_2) than these standard benchmarks.

E. Benchmark Generation Algorithm

Initialization: Policy parameters
Input: Validation set, number of iterations $MAX_{iter} = 3500$
Output: Optimized policy for Dueling DQN

image **in** validation set Load the image Calculate reward R_t and advantage A_t based on current value function Calculate sensitivity of ground truth classification probability P_{GT} to change in

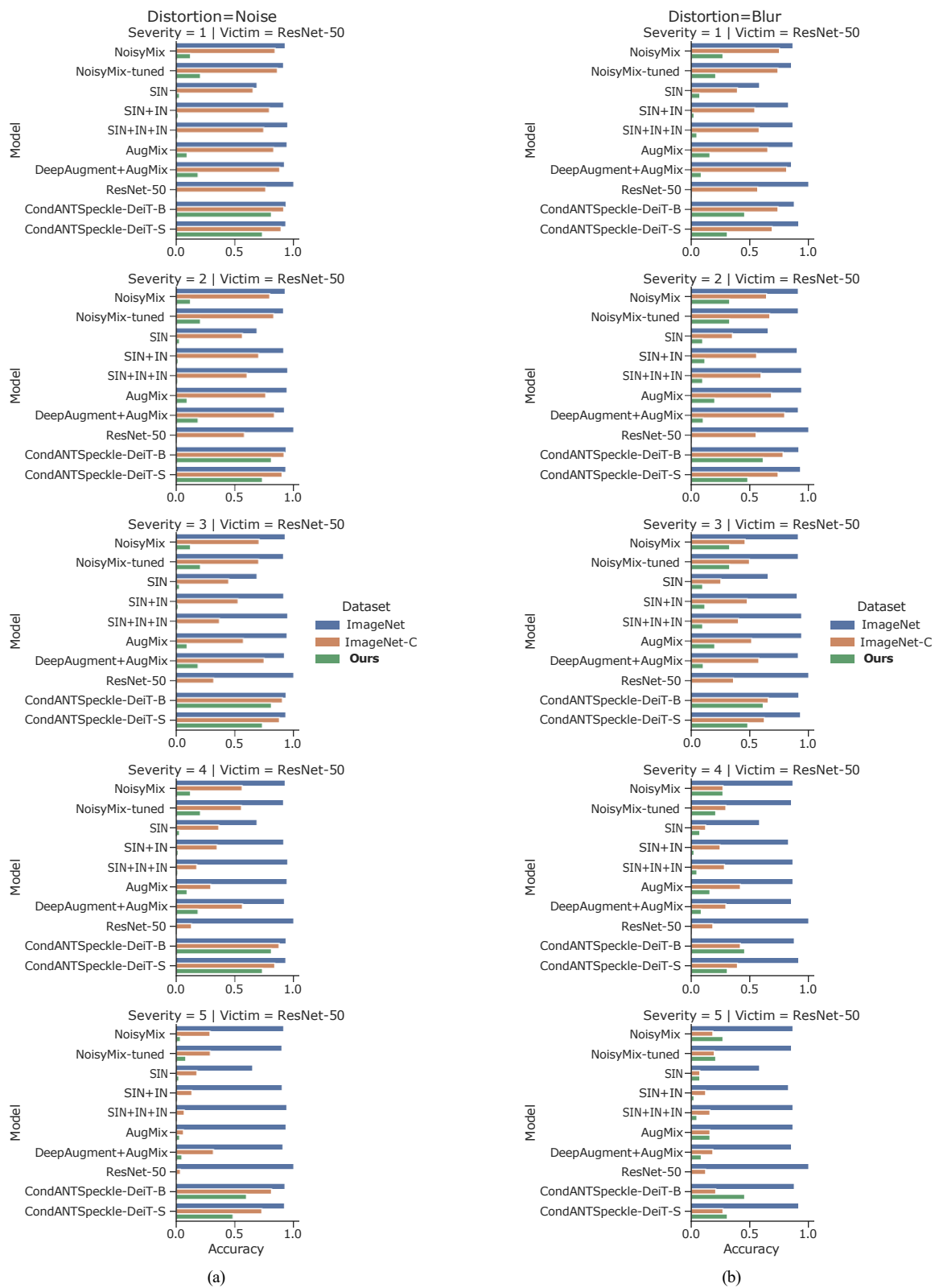


Figure 8. Robustness method scores on ImageNet, ImageNet-C, and our distorted version of ImageNet across all severity levels for the (a) Gaussian noise and (b) blur distortions. The robustness methods perform worse on our split.

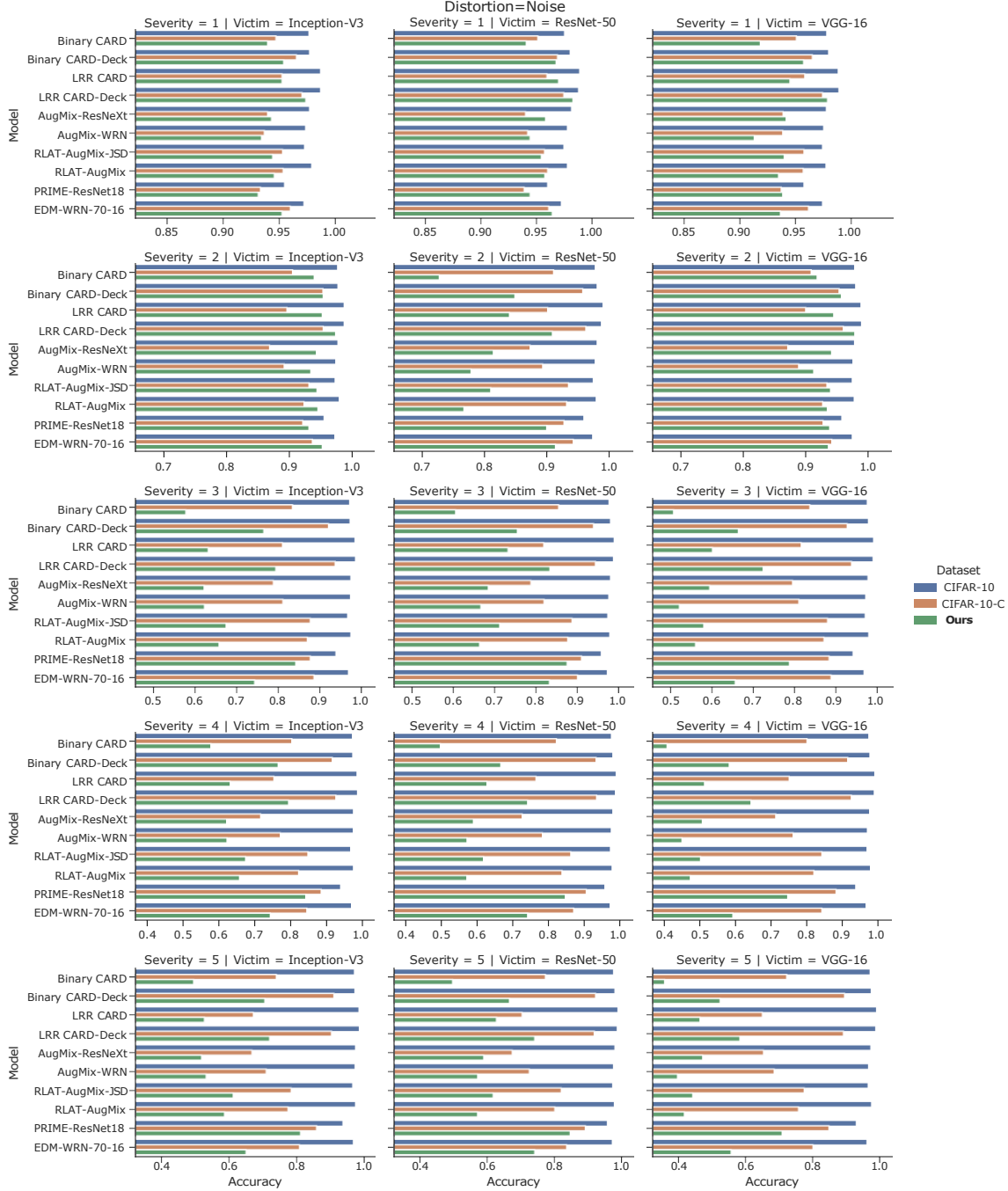


Figure 9. Robustness method scores on CIFAR-10, CIFAR-10-C, and our distorted version of CIFAR-10 across all severity levels for the Gaussian noise distortion. Across the Inception-V3 and ResNet-50 victim models, robustness methods perform worse on our split on average.

distortion for square patches $i \leftarrow 0$ $Pred_{fstep} \leftarrow 1 - P_{GT}$
 $Pred_{GT} == Pred_{fstep}$ and $i < Max_{iter}$ Collect the set of trajectories (state, action) by running policy $\pi_k = \pi(\theta_k)$ in the environment \rightarrow action ($N_{add\ dist}$, $N_{rem\ dist}$) Generate adversarial image x' with respect to the distortion type and the chosen patch (i.e., select the action and take the action) Calculate reward

R_t and TD error Update the the RL network policy Perform prediction on $x' \rightarrow Pred_{fstep}$ $i \leftarrow i + 1$

Algorithm E shows the pipelines for benchmark generation.

F. Dataset Information

ImageNet The ImageNet dataset [8] is provided contingent on terms that are specified on the [ImageNet website](#). It is known that ImageNet contains web-scraped images containing people without their consent, which can be considered to contain personally identifiable information.

ImageNet-C The ImageNet-C dataset [17] has a Creative Commons Attribution 4.0 International license. It is known that ImageNet (and in turn its derivatives) contains web-scraped images containing people without their consent, which can be considered to contain personally identifiable information.

CIFAR-10 The CIFAR-10 dataset [22] is provided without a license.

CIFAR-10-C The CIFAR-10-C dataset [17] has a Creative Commons Attribution 4.0 International license.

G. Accessibility, Documentation, and License

Our dataset documentation can be found at <https://<redacted>.github.io/<redacted>> and code at <https://github.com/<redacted>>. The documentation includes how to load the generated data. We use Zenodo to associate a DOI with the repository. There is schema.org structured metadata provided on the website as well. The benchmark is made available under the MIT license, which is included with the GitHub repository.

We plan to continue hosting the benchmark through GitHub as-is and provide maintenance as necessary. We the authors bear all responsibility in case of violation of rights, etc.

H. Experimental Details

ImageNet Experiments on ImageNet use its validation set of 50,000 samples. For robustness experiments involving RobustBench, the only preprocessing done is to scale the pixel values by 255 so that values lie between 0 and 1, as is standard for the pretrained models in RobustBench [4]. For other experiments, z-score normalization is applied with statistics taken from the train split.

ImageNet-C Experiments on ImageNet-C use its validation set of 10,000 samples. The ImageNet-C distortions do not include Gaussian blur, however, it does contain various types of blur. In experiments, we compare results on Gaussian blur distortion in our framework to defocus blur in ImageNet-C, which are more similar than the motion, glass, or zoom blurs. For robustness experiments involving RobustBench, the only preprocessing done is to scale the

pixel values by 255 so that values lie between 0 and 1, as is standard for the pretrained models in RobustBench [4]. For other experiments, z-score normalization is applied with statistics taken from the train split. In RobustBench, there is a **subset** of the validation splits comprising 5,000 samples that is used for evaluation, rather than all 50,000.

ImageNet-Ours ImageNet-Ours follows the same train, validation, and test splits as the original ImageNet dataset [8]. The distortions in the dataset are generated on the validation split of ImageNet.

We provide this dataset on Zenodo: <https://zenodo.org/<redacted>>

For all our experiments, we used a patch size of 8×8 and the patches were non-overlapping to reduce the action space. We observed that increasing the size of the patch eventually increased the L_2 while it decreased the total number of steps to generate the adversarial sample. As we had a bound on the L_2 , using the patch size of 8×8 gave us favorable results. The noise intensity level 1 is assumed to be the adversarial sample at the time of misclassification. We further increase the noise level by $2\times$, $3\times$, $4\times$, and $5\times$ the noise at level 1 for the experiments.

CIFAR-10 We use the standard CIFAR-10 train and test splits [22]. Experiments on CIFAR-10 use its test set of 10,000 samples. For robustness experiments involving RobustBench, the only preprocessing done is to scale the pixel values by 255 so that values lie between 0 and 1, as is standard for the pretrained models in RobustBench [4]. For other experiments, z-score normalization is applied with statistics taken from the train split.

CIFAR-10-C CIFAR-10-C follows the same train and test splits as the original CIFAR-10 dataset [22]. Experiments on CIFAR-10-C use its distorted versions of the CIFAR-10 test set, each of which is 10,000 samples. There is one such test set for five distortion levels and various types of distortions (corruptions), which contains the same corruptions that we apply in our framework – the results on these splits can be compared directly. For robustness experiments involving RobustBench, the only preprocessing done is to scale the pixel values by 255 so that values lie between 0 and 1, as is standard for the pretrained models in RobustBench [4]. For other experiments, z-score normalization is applied with statistics taken from the train split.

CIFAR-10-Ours CIFAR-10-Ours follows the same train and test splits as the original CIFAR-10 dataset [22]. The distortions in the dataset are generated on the test split of CIFAR-10.

We provide this dataset on Zenodo: <https://zenodo.org/<redacted>>.

For all our experiments, we used a patch size of 2×2 and the patches were non-overlapping to reduce the action space. We observed that increasing the size of the patch eventually increased the L_2 while it decreased the total number of steps to generate the adversarial sample. As we had a bound on the L_2 , using the smallest patch size of 2×2 gave us favorable results. The noise intensity level 1 is assumed to be the adversarial sample at the time of misclassification. We further increase the noise level by $2\times$, $3\times$, $4\times$, and $5\times$ the noise at level 1 for the experiments.

Comparing Our Distorted Datasets with CIFAR-10-C/ImageNet-C For a fair comparison, we compute the average L_2 distance (listed in main text) between the original test/validation sets and the CIFAR-10-C/ImageNet-C test/validation sets for each type of distortion. We then employ our framework to generate distorted versions of those data splits for the approximate average L_2 of each CIFAR-10-C/ImageNet-C severity. Due to our sample generation procedure, we do not set a target L_2 (nor do the generators of CIFAR-10-C/ImageNet-C) so we must approximate the target average L_2 . In experiments, we set generation parameters empirically and keep splits that have an average L_2 of within 25%. Often, especially with Gaussian blur, our average L_2 is far lower than that of CIFAR-10-C/ImageNet-C. For instance, the mean L_2 level of ImageNet-C (99.3) is 69.0% higher than the mean L_2 level on our distorted version of ImageNet (58.8) for Gaussian noise, yet we cause greater accuracy degradation for robustness models.

We also perform a fair sample wise comparison such that harder samples are not excluded or easier samples are not included by one split or another. This is done by storing the indices of every sample in each split, including the original split, CIFAR-10-C/ImageNet-C split, and our split. The intersection between these three sets of indices is used for evaluation. To reiterate, this prevents sample difficulty from inflating or deflating accuracy between splits.

Standard Models We evaluated the performance of standard models such as VGG-16 [45], Inception-v3, and ResNet-50 [15, 46] and evaluated them against data generated with our adversarial generator. Table 2 in the main text shows the evaluation results across standard models as victims.

Robustness Models All robustness methods are available through the **RobustBench** [4] library. This includes their software licenses, neural network parameters, and neural network architectures implemented in `PyTorch` [30]. To select which robustness models to use, we evaluated every single available model (all threat models) on both CIFAR-10-C and ImageNet-C – this was done as not all models

were evaluated on all RobustBench benchmarks. The top-10, as evaluated by the mean accuracy across all five severities on each of CIFAR-10-C and ImageNet-C, were selected to evaluate on our generated benchmarks. Citations for each selected method are present in the main text. We consider these to be the state-of-the-art as RobustBench is reputable and continuously updated.

I. Compute Resources

Experiments were conducted on a single machine within an internal cluster. The machine contains eight NVIDIA Tesla V100 32GB GPUs, 756GB of DDR4 2933 MT/s RAM, and an Intel(R) Xeon(R) Gold 6248 CPU @ 2.50GHz (2 sockets, 2 cores/socket, and 2 threads/core for a total of 80 logical cores).

J. Software Libraries

This work was made possible with the RobustBench [4] (MIT License), PyTorch [30] (BSD-Style), seaborn [51] (BSD 3-Clause), pandas [29] (BSD 3-Clause License), matplotlib [19] (Various Licenses), and jupyter [21] (BSD 3-Clause License) libraries for Python [48] (PSF License).

K. Other Reproducibility Details

The code is seeded for reproducibility and contains every seed used. For experiments involving RobustBench, all model architectures and weights are available for download through the RobustBench [4] library. The remaining reproducibility information is detailed in the other sections of this document.

L. Complete Benchmark Results

We include tables of every single model evaluated in our study for both CIFAR-10 and ImageNet. Please see the tables following the references.

Distortion	Victim Model	Dataset Model ID	Ours	ImageNet	ImageNet-C
Blur	ResNet-50	AlexNet	0.2232	0.5146	0.1280
		Erichson2022NoisyMix	0.4307	0.8750	0.4825
		Erichson2022NoisyMix_new	0.4018	0.8946	0.4982
		Geirhos2018_SIN	0.2146	0.6199	0.2512
		Geirhos2018_SIN_JN	0.2583	0.8542	0.4192
		Geirhos2018_SIN_JN_JN	0.2699	0.8794	0.4091
		Hendrycks2020AugMix	0.3654	0.8870	0.5162
		Hendrycks2020Many	0.2894	0.8719	0.5486
		Salman2020Do_50_2_Linf	0.3801	0.6867	0.2349
		Standard_R50	0.0000	1.0000	0.3794
		Tian2022Deeper_DeiT-B	0.5966	0.8801	0.5735
		Tian2022Deeper_DeiT-S	0.5191	0.9105	0.5613

Table 4. All ImageNet accuracy scores for the Blur distortion and the victim model ResNet-50.

Distortion	Victim Model	Dataset Model ID	Ours	ImageNet	ImageNet-C
Noise	ResNet-50	AlexNet	0.1932	0.6756	0.1254
		Erichson2022NoisyMix	0.3595	0.9251	0.6477
		Erichson2022NoisyMix_new	0.4180	0.9107	0.6566
		Geirhos2018_SIN	0.1662	0.6850	0.4467
		Geirhos2018_SIN_JN	0.2321	0.9136	0.5038
		Geirhos2018_SIN_JN_JN	0.2277	0.9482	0.3928
		Hendrycks2020AugMix	0.3277	0.9424	0.5075
		Hendrycks2020Many	0.3697	0.9194	0.6786
		Salman2020Do_50_2_Linf	0.2586	0.7964	0.3117
		Standard_R50	0.0000	1.0000	0.3660
		Tian2022Deeper_DeiT-B	0.8167	0.9338	0.8903
		Tian2022Deeper_DeiT-S	0.7553	0.9309	0.8555

Table 5. All ImageNet accuracy scores for the Noise distortion and the victim model ResNet-50.

Distortion	Victim Model	Dataset Model ID	Ours	CIFAR-10	CIFAR-10-C
Blur	Inception-V3	Addepalli2021Towards_RN18	0.5638	0.6333	0.5618
		AGAT [13]	0.2723	0.7382	0.6408
		Addepalli2021Towards_WRN34	0.5515	0.5989	0.5618
		Addepalli2022Efficient_RN18	0.5814	0.6279	0.5906
		Addepalli2022Efficient_WRN_34_10	0.6442	0.6921	0.6228
		Andriushchenko2020Understanding	0.4899	0.5467	0.4871
		Augustin2020Adversarial	0.6963	0.7941	0.7257
		Augustin2020Adversarial_34_10	0.7234	0.8170	0.7102
		Augustin2020Adversarial_34_10_extra	0.7268	0.8571	0.7904
		Carmon2019Unlabeled	0.5893	0.7265	0.6288
		Chen2020Adversarial	0.6118	0.5943	0.5858
		Chen2020Efficient	0.5519	0.6257	0.5834
		Chen2021LTD_WRN34_10	0.5804	0.6309	0.5665
		Chen2021LTD_WRN34_20	0.6172	0.6715	0.5929
		Cui2020Learnable_34_10	0.6444	0.6688	0.6388
		Cui2020Learnable_34_20	0.6051	0.6367	0.6100
		Dai2021Parameterizing	0.5960	0.6838	0.5880
		Debenedetti2022Light_XCIT-L12	0.6667	0.7148	0.6699
		Debenedetti2022Light_XCIT-M12	0.6549	0.7211	0.6599
		Debenedetti2022Light_XCIT-S12	0.6458	0.6960	0.6301
		Diffenderfer2021Winning_Binary	0.5088	0.8770	0.8185
		Diffenderfer2021Winning_Binary_CARD_Deck	0.6158	0.8933	0.8129
		Diffenderfer2021Winning_LRR	0.5735	0.8830	0.8756
		Diffenderfer2021Winning_LRR_CARD_Deck	0.6538	0.9263	0.8484
		Ding2020MMA	0.5873	0.6492	0.5769
		Engstrom2019Robustness	0.6995	0.8019	0.6855
		Gowal2020Uncovering	0.6728	0.7533	0.6838
		Gowal2020Uncovering_28_10_extra	0.6213	0.7092	0.6246
		Gowal2020Uncovering_34_20	0.5401	0.6164	0.5698
		Gowal2020Uncovering_70_16	0.5753	0.6429	0.5850
		Gowal2020Uncovering_70_16_extra	0.6293	0.7378	0.6251
		Gowal2020Uncovering_extra	0.7661	0.8930	0.7805
		Gowal2021Improving_28_10_ddpm_100m	0.6565	0.7039	0.6406
		Gowal2021Improving_70_16_ddpm_100m	0.6601	0.7105	0.6553
		Gowal2021Improving_R18_ddpm_100m	0.6300	0.6743	0.6231
		Hendrycks2019Using	0.5486	0.6242	0.5549
		Hendrycks2020AugMix_ResNeXt	0.5853	0.8259	0.8462
		Hendrycks2020AugMix_WRN	0.5450	0.8728	0.8207
		Huang2020Self	0.5707	0.6407	0.5783
		Huang2021Exploring	0.6460	0.7403	0.6818
		Huang2021Exploring_ema	0.6855	0.8141	0.6951
		Huang2022Revisiting_WRN-A4	0.6667	0.8182	0.6964
		Jia2022LAS-AT_34_10	0.6181	0.6649	0.5943
		Jia2022LAS-AT_70_16	0.6218	0.6764	0.6152
		Kang2021Stable	0.7161	0.8240	0.7176
		Kireev2021Effectiveness_AugMixNoJSD	0.5177	0.8734	0.8172
		Kireev2021Effectiveness_Gauss50percent	0.6350	0.8585	0.7602
		Kireev2021Effectiveness_RLAT	0.6537	0.8053	0.7099
		Kireev2021Effectiveness_RLATAugMix	0.6319	0.8608	0.8241
		Kireev2021Effectiveness_RLATAugMixNoJSD	0.6034	0.8983	0.8522
		Modas2021PRIMEResNet18	0.6212	0.7549	0.7434
		Pang2020Boosting	0.5764	0.6558	0.5946
		Pang2022Robustness_WRN28_10	0.6207	0.6792	0.5975
		Pang2022Robustness_WRN70_16	0.5985	0.6586	0.6046
		Rade2021Helper_R18_ddpm	0.6436	0.7489	0.6396
		Rade2021Helper_R18_extra	0.6022	0.6813	0.6276
		Rade2021Helper_ddpm	0.6497	0.6887	0.6357
		Rade2021Helper_extra	0.7034	0.8171	0.7049
		Rebuffi2021Fixing_106_16_cutmix_ddpm	0.6285	0.6931	0.6197
		Rebuffi2021Fixing_28_10_cutmix_ddpm	0.6632	0.7643	0.6584
		Rebuffi2021Fixing_70_16_cutmix_ddpm	0.7032	0.7876	0.6797
		Rebuffi2021Fixing_70_16_cutmix_extra	0.7857	0.8902	0.8009
		Rebuffi2021Fixing_70_16_cutmix_extra_L2	0.7857	0.8902	0.8009
		Rebuffi2021Fixing_70_16_cutmix_extra_Linf	0.6582	0.8032	0.6929
		Rebuffi2021Fixing_R18_cutmix_ddpm	0.6311	0.7067	0.6548
		Rebuffi2021Fixing_R18_ddpm	0.5518	0.6140	0.5590
		Rice2020Overfitting	0.6243	0.7074	0.5956
Rony2019Decoupling	0.6779	0.7773	0.6535		
Schwag2020Hydra	0.5841	0.6756	0.6009		
Schwag2021Proxy	0.6688	0.7279	0.6791		
Schwag2021Proxy_R18	0.6730	0.7021	0.6586		
Schwag2021Proxy_ResNest152	0.6098	0.6445	0.5890		
Sitawarin2020Improving	0.5501	0.6599	0.6011		
Sridhar2021Robust	0.5961	0.6798	0.6345		
Sridhar2021Robust_34_15	0.6059	0.6931	0.6179		
Standard	0.3487	0.8632	0.6693		
Wang2020Improving	0.5952	0.6722	0.6002		
Wang2023Better_WRN-28-10	0.7832	0.8562	0.7968		
Wang2023Better_WRN-70-16	0.7837	0.8560	0.7881		
Wong2020Fast	0.5931	0.6554	0.5630		
Wu2020Adversarial	0.6630	0.7294	0.6588		
Wu2020Adversarial_extra	0.5805	0.6305	0.5964		
Xu2023Exploring_WRN-28-10	0.7296	0.8124	0.7378		
Zhang2019Theoretically	0.5509	0.6169	0.5499		
Zhang2019You	0.6186	0.6466	0.6169		
Zhang2020Attacks	0.6206	0.6867	0.5899		
Zhang2020Geometry	0.6227	0.7257	0.6638		

Table 6. All CIFAR-10 accuracy scores for the Blur distortion and the victim model Inception-V3.

Distortion	Victim Model	Dataset Model ID	Ours	CIFAR-10	CIFAR-10-C
Blur	ResNet-50	Addepalli2021Towards_RN18	0.5787	0.6462	0.6403
		AGAT	0.2843	0.6679	0.6725
		Addepalli2021Towards_WRN34	0.6462	0.7154	0.6770
		Addepalli2022Efficient_RN18	0.6294	0.6822	0.6604
		Addepalli2022Efficient_WRN_34_10	0.6741	0.7707	0.6992
		Andriushchenko2020Understanding	0.5427	0.6163	0.5930
		Augustin2020Adversarial	0.6715	0.7490	0.7106
		Augustin2020Adversarial_34_10	0.6981	0.7928	0.7301
		Augustin2020Adversarial_34_10_extra	0.7174	0.8186	0.7798
		Carmon2019Unlabeled	0.6888	0.7757	0.7336
		Chen2020Adversarial	0.6452	0.6590	0.6981
		Chen2020Efficient	0.6275	0.6525	0.6725
		Chen2021LTD_WRN34_10	0.6335	0.6590	0.6433
		Chen2021LTD_WRN34_20	0.6770	0.7485	0.6880
		Cui2020Learnable_34_10	0.6551	0.7490	0.6804
		Cui2020Learnable_34_20	0.5978	0.7309	0.6874
		Dai2021Parameterizing	0.6247	0.7609	0.7237
		Debenedetti2022Light_XCIT-L12	0.6981	0.8271	0.7362
		Debenedetti2022Light_XCIT-M12	0.7070	0.8008	0.7332
		Debenedetti2022Light_XCIT-S12	0.6837	0.7475	0.7023
		Diffenderfer2021Winning_Binary	0.4640	0.8331	0.7926
		Diffenderfer2021Winning_Binary_CARD_Deck	0.5066	0.8334	0.8310
		Diffenderfer2021Winning_LRR	0.5968	0.9364	0.9066
		Diffenderfer2021Winning_LRR_CARD_Deck	0.6214	0.8914	0.8589
		Ding2020MMA	0.7105	0.7475	0.7248
		Engstrom2019Robustness	0.7059	0.8071	0.7588
		Gowal2020Uncovering	0.6921	0.7851	0.7473
		Gowal2020Uncovering_28_10_extra	0.7043	0.7828	0.7314
		Gowal2020Uncovering_34_20	0.6239	0.6977	0.6705
		Gowal2020Uncovering_70_16	0.5895	0.6824	0.6659
		Gowal2020Uncovering_70_16_extra	0.6673	0.7949	0.7340
		Gowal2020Uncovering_extra	0.7446	0.8397	0.8021
		Gowal2021Improving_28_10_ddpm_100m	0.6372	0.7531	0.7049
		Gowal2021Improving_70_16_ddpm_100m	0.6492	0.7795	0.7472
		Gowal2021Improving_R18_ddpm_100m	0.6448	0.7413	0.7013
		Hendrycks2019Using	0.6047	0.6980	0.6467
		Hendrycks2020AugMix_ResNeXt	0.5290	0.8900	0.8686
		Hendrycks2020AugMix_WRN	0.4582	0.8427	0.8323
		Huang2020Self	0.5931	0.7307	0.6873
		Huang2021Exploring	0.7064	0.7769	0.7414
		Huang2021Exploring_ema	0.7144	0.8171	0.7735
		Huang2022Revisiting_WRN-A4	0.6876	0.8077	0.7603
		Jia2022LAS-AT_34_10	0.5886	0.6375	0.6137
		Jia2022LAS-AT_70_16	0.6714	0.7642	0.7025
		Kang2021Stable	0.7477	0.8424	0.7965
		Kireev2021Effectiveness_AugMixNoJSD	0.4208	0.9261	0.8850
		Kireev2021Effectiveness_Gauss50percent	0.4967	0.8489	0.7755
		Kireev2021Effectiveness_RLAT	0.5867	0.7970	0.7477
		Kireev2021Effectiveness_RLATAugMix	0.5535	0.8804	0.8560
		Kireev2021Effectiveness_RLATAugMixNoJSD	0.4995	0.9102	0.8807
		Modas2021PRIMEResNet18	0.5925	0.7984	0.7706
		Pang2020Boosting	0.5997	0.6891	0.6460
		Pang2022Robustness_WRN28_10	0.6289	0.7560	0.6996
		Pang2022Robustness_WRN70_16	0.6569	0.7384	0.6960
		Rade2021Helper_R18_ddpm	0.6901	0.7827	0.7440
		Rade2021Helper_R18_extra	0.6695	0.7727	0.7273
		Rade2021Helper_ddpm	0.6564	0.7796	0.7247
		Rade2021Helper_extra	0.7126	0.8112	0.7597
		Rebuffi2021Fixing_106_16_cutmix_ddpm	0.6159	0.7851	0.7152
		Rebuffi2021Fixing_28_10_cutmix_ddpm	0.6900	0.8035	0.7405
		Rebuffi2021Fixing_70_16_cutmix_ddpm	0.7112	0.8332	0.7755
		Rebuffi2021Fixing_70_16_cutmix_extra	0.7386	0.8628	0.8205
		Rebuffi2021Fixing_70_16_cutmix_extra_L2	0.7386	0.8628	0.8205
		Rebuffi2021Fixing_70_16_cutmix_extra_Linf	0.6931	0.8055	0.7644
		Rebuffi2021Fixing_R18_cutmix_ddpm	0.6588	0.7526	0.7133
		Rebuffi2021Fixing_R18_ddpm	0.5824	0.7292	0.6685
		Rice2020Overfitting	0.6355	0.7161	0.6890
		Rony2019Decoupling	0.6919	0.7980	0.7377
		Schwag2020Hydra	0.6872	0.7389	0.7033
		Schwag2021Proxy	0.6722	0.7739	0.7254
		Schwag2021Proxy_R18	0.6674	0.7341	0.6976
		Schwag2021Proxy_ResNest152	0.6405	0.7231	0.6984
		Sitawarin2020Improving	0.6529	0.7742	0.7014
Sridhar2021Robust	0.6850	0.7685	0.7329		
Sridhar2021Robust_34_15	0.6398	0.7593	0.7041		
Standard	0.2418	0.8078	0.7419		
Wang2020Improving	0.6361	0.7356	0.6852		
Wang2023Better_WRN-28-10	0.7341	0.8520	0.8157		
Wang2023Better_WRN-70-16	0.7449	0.8555	0.7941		
Wong2020Fast	0.6208	0.6626	0.6458		
Wu2020Adversarial	0.6597	0.7541	0.7046		
Wu2020Adversarial_extra	0.6621	0.7926	0.7263		
Xu2023Exploring_WRN-28-10	0.7053	0.7963	0.7625		
Zhang2019Theoretically	0.6080	0.6830	0.6418		
Zhang2019You	0.6373	0.6896	0.6554		
Zhang2020Attacks	0.6029	0.7498	0.7136		
Zhang2020Geometry	0.7156	0.7993	0.7418		

Table 7. All CIFAR-10 accuracy scores for the Blur distortion and the victim model ResNet-50.

Distortion	Victim Model	Dataset Model ID	Ours	CIFAR-10	CIFAR-10-C
Blur	VGG-16	Addepalli2021Towards_RN18	0.5412	0.6179	0.5658
		AGAT	0.2374	0.6565	0.6120
		Addepalli2021Towards_WRN34	0.5889	0.6795	0.6195
		Addepalli2022Efficient_RN18	0.5944	0.6602	0.6014
		Addepalli2022Efficient_WRN_34_10	0.6192	0.7093	0.6444
		Andriushchenko2020Understanding	0.5234	0.5857	0.5236
		Augustin2020Adversarial	0.6651	0.7670	0.7064
		Augustin2020Adversarial_34_10	0.7191	0.7910	0.7405
		Augustin2020Adversarial_34_10_extra	0.7601	0.8733	0.8176
		Carmon2019Unlabeled	0.6636	0.7521	0.6832
		Chen2020Adversarial	0.5877	0.6439	0.5914
		Chen2020Efficient	0.5809	0.6484	0.6043
		Chen2021LTD_WRN34_10	0.5955	0.6613	0.5980
		Chen2021LTD_WRN34_20	0.5780	0.6561	0.5975
		Cui2020Learnable_34_10	0.6285	0.7132	0.6462
		Cui2020Learnable_34_20	0.6121	0.6906	0.6244
		Dai2021Parameterizing	0.6021	0.7002	0.6271
		Debenedetti2022Light_XCIT-L12	0.7209	0.7690	0.7265
		Debenedetti2022Light_XCIT-M12	0.7160	0.8015	0.7144
		Debenedetti2022Light_XCIT-S12	0.6590	0.7338	0.6808
		Diffenderfer2021Winning_Binary	0.5221	0.9024	0.8712
		Diffenderfer2021Winning_Binary_CARD_Deck	0.5582	0.9030	0.8358
		Diffenderfer2021Winning_LRR	0.5413	0.9738	0.9305
		Diffenderfer2021Winning_LRR_CARD_Deck	0.5924	0.9477	0.9019
		Ding2020MMA	0.6053	0.6799	0.6201
		Engstrom2019Robustness	0.7022	0.7749	0.6918
		Gowal2020Uncovering	0.6544	0.7426	0.6793
		Gowal2020Uncovering_28_10_extra	0.6561	0.7306	0.6747
		Gowal2020Uncovering_34_20	0.5833	0.6442	0.5966
		Gowal2020Uncovering_70_16	0.5659	0.6493	0.5830
		Gowal2020Uncovering_70_16_extra	0.6999	0.7822	0.7219
		Gowal2020Uncovering_extra	0.7721	0.8843	0.8172
		Gowal2021Improving_28_10_ddpm_100m	0.6478	0.7092	0.6608
		Gowal2021Improving_70_16_ddpm_100m	0.6522	0.7375	0.6806
		Gowal2021Improving_R18_ddpm_100m	0.6089	0.6802	0.6371
		Hendrycks2019Using	0.6072	0.6930	0.6272
		Hendrycks2020AugMix_ResNeXt	0.5406	0.8975	0.8630
		Hendrycks2020AugMix_WRN	0.4770	0.8780	0.8525
		Huang2020Self	0.5572	0.6062	0.5613
		Huang2021Exploring	0.6637	0.7647	0.7051
		Huang2021Exploring_ema	0.7054	0.8025	0.7271
		Huang2022Revisiting_WRN-A4	0.7012	0.8210	0.7471
		Jia2022LAS-AT_34_10	0.5871	0.6703	0.6058
		Jia2022LAS-AT_70_16	0.5973	0.6705	0.6055
		Kang2021Stable	0.7573	0.8689	0.7857
		Kireev2021Effectiveness_AugMixNoJSD	0.3979	0.8829	0.8634
		Kireev2021Effectiveness_Gauss50percent	0.4847	0.7835	0.6981
		Kireev2021Effectiveness_RLAT	0.5897	0.7663	0.6966
		Kireev2021Effectiveness_RLATAugMix	0.5559	0.8902	0.8433
		Kireev2021Effectiveness_RLATAugMixNoJSD	0.5609	0.9076	0.8846
		Modas2021PRIMEResNet18	0.6117	0.8340	0.7868
		Pang2020Boosting	0.5760	0.6680	0.6186
		Pang2022Robustness_WRN28_10	0.6143	0.6813	0.6170
		Pang2022Robustness_WRN70_16	0.6177	0.6862	0.6357
		Rade2021Helper_R18_ddpm	0.6942	0.7941	0.7122
		Rade2021Helper_R18_extra	0.6698	0.7373	0.6841
		Rade2021Helper_ddpm	0.6293	0.6954	0.6279
		Rade2021Helper_extra	0.7028	0.8141	0.7337
		Rebuffi2021Fixing_106_16_cutmix_ddpm	0.6341	0.7082	0.6471
		Rebuffi2021Fixing_28_10_cutmix_ddpm	0.6941	0.7918	0.7372
Rebuffi2021Fixing_70_16_cutmix_ddpm	0.7128	0.8288	0.7487		
Rebuffi2021Fixing_70_16_cutmix_extra	0.7712	0.8946	0.8378		
Rebuffi2021Fixing_70_16_cutmix_extra_L2	0.7712	0.8946	0.8378		
Rebuffi2021Fixing_70_16_cutmix_extra_Linf	0.6976	0.8036	0.7351		
Rebuffi2021Fixing_R18_cutmix_ddpm	0.6510	0.7524	0.6823		
Rebuffi2021Fixing_R18_ddpm	0.5713	0.6213	0.5761		
Rice2020Overfitting	0.6150	0.6795	0.6213		
Rony2019Decoupling	0.6693	0.7484	0.6331		
Schwag2020Hydra	0.6492	0.7318	0.6662		
Schwag2021Proxy	0.6777	0.7707	0.7200		
Schwag2021Proxy_R18	0.6349	0.7342	0.6901		
Schwag2021Proxy_ResNest152	0.6273	0.7121	0.6473		
Sitawarin2020Improving	0.6099	0.6998	0.6209		
Sridhar2021Robust	0.6558	0.7387	0.6777		
Sridhar2021Robust_34_15	0.6334	0.7243	0.6520		
Standard	0.3404	0.9069	0.6913		
Wang2020Improving	0.6427	0.7102	0.6592		
Wang2023Better_WRN-28-10	0.7675	0.8816	0.8151		
Wang2023Better_WRN-70-16	0.7811	0.8964	0.8355		
Wong2020Fast	0.5707	0.6355	0.5485		
Wu2020Adversarial	0.6445	0.7189	0.6348		
Wu2020Adversarial_extra	0.6470	0.7191	0.6573		
Xu2023Exploring_WRN-28-10	0.6971	0.8504	0.7632		
Zhang2019Theoretically	0.5936	0.6719	0.6101		
Zhang2019You	0.6417	0.6987	0.6370		
Zhang2020Attacks	0.5806	0.6692	0.6049		
Zhang2020Geometry	0.6456	0.7567	0.6814		

Table 8. All CIFAR-10 accuracy scores for the Blur distortion and the victim model VGG-16.

Distortion	Victim Model	Dataset Model ID	Ours	CIFAR-10	CIFAR-10-C
Noise	Inception-V3	Addepalli2021Towards_RN18	0.5686	0.8136	0.7618
		AGAT	0.3567	0.8616	0.6471
		Addepalli2021Towards_WRN34	0.5099	0.8475	0.7625
		Addepalli2022Efficient_RN18	0.5910	0.8551	0.8085
		Addepalli2022Efficient_WRN_34_10	0.6364	0.8839	0.8337
		Andriushchenko2020Understanding	0.5323	0.7919	0.7497
		Augustin2020Adversarial	0.5555	0.9222	0.7916
		Augustin2020Adversarial_34_10	0.5935	0.9295	0.8258
		Augustin2020Adversarial_34_10_extra	0.6076	0.9468	0.8788
		Carmon2019Unlabeled	0.6106	0.8994	0.8217
		Chen2020Adversarial	0.5499	0.8513	0.7972
		Chen2020Efficient	0.5917	0.8473	0.7938
		Chen2021LTD_WRN34_10	0.6070	0.8512	0.7947
		Chen2021LTD_WRN34_20	0.5998	0.8599	0.7988
		Cui2020Learnable_34_10	0.6292	0.8799	0.8233
		Cui2020Learnable_34_20	0.5917	0.8792	0.8267
		Dai2021Parameterizing	0.6290	0.8675	0.8059
		Debenedetti2022Light_XCIT-L12	0.6413	0.9106	0.8467
		Debenedetti2022Light_XCIT-M12	0.6241	0.9062	0.8334
		Debenedetti2022Light_XCIT-S12	0.6065	0.8929	0.8356
		Diffenderfer2021Winning_Binary	0.5265	0.9696	0.8359
		Diffenderfer2021Winning_Binary_CARD_Deck	0.6777	0.9706	0.9269
		Diffenderfer2021Winning_LRR	0.5475	0.9832	0.8098
		Diffenderfer2021Winning_LRR_CARD_Deck	0.6867	0.9841	0.9337
		Ding2020MMA	0.6246	0.8872	0.8382
		Engstrom2019Robustness	0.6445	0.9213	0.8651
		Gowal2020Uncovering	0.7190	0.9226	0.8875
		Gowal2020Uncovering_28_10_extra	0.6071	0.9006	0.8292
		Gowal2020Uncovering_34_20	0.6049	0.8544	0.8085
		Gowal2020Uncovering_70_16	0.5978	0.8543	0.8087
		Gowal2020Uncovering_70_16_extra	0.6282	0.9153	0.8358
		Gowal2020Uncovering_extra	0.6189	0.9637	0.8878
		Gowal2021Improving_28_10_ddpm_100m	0.5713	0.8816	0.8022
		Gowal2021Improving_70_16_ddpm_100m	0.5980	0.8880	0.8050
		Gowal2021Improving_R18_ddpm_100m	0.5971	0.8724	0.8246
		Hendrycks2019Using	0.5366	0.8728	0.7805
		Hendrycks2020AugMix_ResNeXt	0.5499	0.9724	0.7871
		Hendrycks2020AugMix_WRN	0.5472	0.9710	0.8170
		Huang2020Self	0.5872	0.8309	0.7837
		Huang2021Exploring	0.6494	0.9108	0.8263
		Huang2021Exploring_ema	0.6144	0.9225	0.8384
		Huang2022Revisiting_WRN-A4	0.6064	0.9207	0.8376
		Jia2022LAS-AT_34_10	0.6006	0.8473	0.7883
		Jia2022LAS-AT_70_16	0.5886	0.8544	0.7973
		Kang2021Stable	0.5620	0.9458	0.8631
		Kireev2021Effectiveness_AugMixNoJSD	0.5093	0.9701	0.7754
		Kireev2021Effectiveness_Gauss50percent	0.6736	0.9483	0.9279
		Kireev2021Effectiveness_RLAT	0.5774	0.9446	0.8718
		Kireev2021Effectiveness_RLATAugMix	0.6016	0.9643	0.8715
		Kireev2021Effectiveness_RLATAugMixNoJSD	0.5980	0.9727	0.8620
		Modas2021PRIMEResNet18	0.8057	0.9357	0.8833
		Pang2020Boosting	0.5679	0.8485	0.7764
		Pang2022Robustness_WRN28_10	0.5754	0.8875	0.8291
		Pang2022Robustness_WRN70_16	0.5871	0.8855	0.8265
		Rade2021Helper_R18_ddpm	0.6644	0.9185	0.8693
		Rade2021Helper_R18_extra	0.4346	0.8906	0.8135
		Rade2021Helper_ddpm	0.5785	0.8838	0.7837
		Rade2021Helper_extra	0.6232	0.9154	0.8456
		Rebuffi2021Fixing_106_16_cutmix_ddpm	0.5645	0.8832	0.8121
		Rebuffi2021Fixing_28_10_cutmix_ddpm	0.5947	0.9197	0.8632
		Rebuffi2021Fixing_70_16_cutmix_ddpm	0.5582	0.8872	0.8157
		Rebuffi2021Fixing_70_16_cutmix_extra	0.5702	0.9286	0.8325
		Rebuffi2021Fixing_70_16_cutmix_extra_L2	0.5665	0.9654	0.8615
		Rebuffi2021Fixing_70_16_cutmix_extra_Linf	0.5702	0.9286	0.8325
		Rebuffi2021Fixing_R18_cutmix_ddpm	0.5947	0.9062	0.8400
		Rebuffi2021Fixing_R18_ddpm	0.5782	0.8316	0.7772
		Rice2020Overfitting	0.6384	0.8896	0.8373
Rony2019Decoupling	0.6673	0.9043	0.8789		
Schwag2020Hydra	0.5996	0.8845	0.8265		
Schwag2021Proxy	0.6686	0.9082	0.8530		
Schwag2021Proxy_R18	0.6419	0.8992	0.8469		
Schwag2021Proxy_ResNest152	0.6088	0.8766	0.8039		
Sitawarin2020Improving	0.5854	0.8750	0.8235		
Sridhar2021Robust	0.6082	0.8964	0.8104		
Sridhar2021Robust_34_15	0.5891	0.8665	0.7879		
Standard	0.3344	0.9745	0.4484		
Wang2020Improving	0.5869	0.8763	0.7961		
Wang2023Better_WRN-28-10	0.6408	0.9292	0.8574		
Wang2023Better_WRN-70-16	0.6428	0.9661	0.8814		
Wong2020Fast	0.5003	0.8348	0.7665		
Wu2020Adversarial	0.6676	0.8828	0.8562		
Wu2020Adversarial_extra	0.6109	0.8838	0.7977		
Xu2023Exploring_WRN-28-10	0.6000	0.9417	0.8705		
Zhang2019Theoretically	0.5925	0.8525	0.7796		
Zhang2019You	0.5869	0.8645	0.8390		
Zhang2020Attacks	0.5745	0.8471	0.7992		
Zhang2020Geometry	0.5815	0.8933	0.8143		

Table 9. All CIFAR-10 accuracy scores for the Noise distortion and the victim model Inception-V3.

Distortion	Victim Model	Dataset Model ID	Ours	CIFAR-10	CIFAR-10-C
Noise	ResNet-50	Addepalli2021Towards_RN18	0.5987	0.8174	0.7752
		AGAT	0.3403	0.8470	0.6424
		Addepalli2021Towards_WRN34	0.6165	0.8704	0.7874
		Addepalli2022Efficient_RN18	0.6528	0.8820	0.8308
		Addepalli2022Efficient_WRN_34_10	0.7058	0.9052	0.8541
		Andriushchenko2020Understanding	0.5710	0.8099	0.7705
		Augustin2020Adversarial	0.6325	0.9323	0.8133
		Augustin2020Adversarial_34_10	0.6765	0.9418	0.8411
		Augustin2020Adversarial_34_10_extra	0.6703	0.9569	0.8896
		Carmon2019Unlabeled	0.6728	0.9122	0.8409
		Chen2020Adversarial	0.6039	0.8766	0.8244
		Chen2020Efficient	0.6371	0.8717	0.8162
		Chen2021LTD_WRN34_10	0.6340	0.8702	0.8135
		Chen2021LTD_WRN34_20	0.6323	0.8789	0.8239
		Cui2020Learnable_34_10	0.6620	0.9016	0.8449
		Cui2020Learnable_34_20	0.6486	0.9022	0.8463
		Dai2021Parameterizing	0.6713	0.8887	0.8295
		Debenedetti2022Light_XCIT-L12	0.7140	0.9301	0.8652
		Debenedetti2022Light_XCIT-M12	0.6939	0.9276	0.8570
		Debenedetti2022Light_XCIT-S12	0.6629	0.9161	0.8542
		Diffenderfer2021Winning_Binary	0.5368	0.9740	0.8550
		Diffenderfer2021Winning_Binary_CARD_Deck	0.6605	0.9782	0.9410
		Diffenderfer2021Winning_LRR	0.6402	0.9877	0.8214
		Diffenderfer2021Winning_LRR_CARD_Deck	0.7214	0.9858	0.9437
		Ding2020MMA	0.6972	0.8988	0.8511
		Engstrom2019Robustness	0.6839	0.9307	0.8813
		Gowal2020Uncovering	0.7776	0.9304	0.8982
		Gowal2020Uncovering_28_10_extra	0.6742	0.9140	0.8469
		Gowal2020Uncovering_34_20	0.6571	0.8755	0.8325
		Gowal2020Uncovering_70_16	0.6371	0.8719	0.8313
		Gowal2020Uncovering_70_16_extra	0.6971	0.9262	0.8537
		Gowal2020Uncovering_extra	0.6859	0.9642	0.9003
		Gowal2021Improving_28_10_ddpm_100m	0.6490	0.8960	0.8262
		Gowal2021Improving_70_16_ddpm_100m	0.6593	0.9095	0.8311
		Gowal2021Improving_R18_ddpm_100m	0.6525	0.8883	0.8401
		Hendrycks2019Using	0.5955	0.8888	0.8019
		Hendrycks2020AugMix_ResNeXt	0.6072	0.9784	0.7904
		Hendrycks2020AugMix_WRN	0.5855	0.9740	0.8238
		Huang2020Self	0.6193	0.8505	0.8067
		Huang2021Exploring	0.6878	0.9241	0.8432
		Huang2021Exploring_ema	0.6856	0.9338	0.8536
		Huang2022Revisiting_WRN-A4	0.6797	0.9317	0.8549
		Jia2022LAS-AT_34_10	0.6395	0.8667	0.8086
		Jia2022LAS-AT_70_16	0.6417	0.8734	0.8231
		Kang2021Stable	0.6223	0.9514	0.8780
		Kireev2021Effectiveness_AugMixNoJSD	0.5075	0.9726	0.7818
		Kireev2021Effectiveness_Gauss50percent	0.6403	0.9548	0.9341
		Kireev2021Effectiveness_RLAT	0.6056	0.9524	0.8833
		Kireev2021Effectiveness_RLATAugMix	0.6296	0.9715	0.8863
		Kireev2021Effectiveness_RLATAugMixNoJSD	0.5820	0.9761	0.8751
		Modas2021PRIMEResNet18	0.8373	0.9549	0.9090
		Pang2020Boosting	0.6165	0.8661	0.7945
		Pang2022Robustness_WRN28_10	0.6369	0.9061	0.8516
		Pang2022Robustness_WRN70_16	0.6445	0.9053	0.8497
		Rade2021Helper_R18_ddpm	0.7358	0.9307	0.8811
		Rade2021Helper_R18_extra	0.5438	0.9037	0.8322
		Rade2021Helper_ddpm	0.6612	0.9002	0.7999
		Rade2021Helper_extra	0.6816	0.9278	0.8627
		Rebuffi2021Fixing_106_16_cutmix_ddpm	0.6313	0.9042	0.8364
		Rebuffi2021Fixing_28_10_cutmix_ddpm	0.6628	0.9386	0.8815
		Rebuffi2021Fixing_70_16_cutmix_ddpm	0.6158	0.9033	0.8389
		Rebuffi2021Fixing_70_16_cutmix_extra	0.6471	0.9690	0.8739
		Rebuffi2021Fixing_70_16_cutmix_extra_L2	0.6471	0.9690	0.8739
		Rebuffi2021Fixing_70_16_cutmix_extra_Linf	0.6431	0.9382	0.8503
		Rebuffi2021Fixing_R18_cutmix_ddpm	0.6811	0.9212	0.8576
		Rebuffi2021Fixing_R18_ddpm	0.6197	0.8557	0.7984
		Rice2020Overfitting	0.6952	0.9043	0.8518
Rony2019Decoupling	0.7091	0.9098	0.8847		
Schwag2020Hydra	0.6723	0.9077	0.8466		
Schwag2021Proxy	0.7222	0.9276	0.8709		
Schwag2021Proxy_R18	0.7019	0.9169	0.8616		
Schwag2021Proxy_ResNest152	0.6812	0.8954	0.8276		
Sitawarin2020Improving	0.6513	0.8874	0.8393		
Sridhar2021Robust	0.6752	0.9131	0.8327		
Sridhar2021Robust_34_15	0.6420	0.8861	0.8066		
Standard	0.3645	0.9708	0.4667		
Wang2020Improving	0.6501	0.8891	0.8153		
Wang2023Better_WRN-28-10	0.6910	0.9398	0.8764		
Wang2023Better_WRN-70-16	0.7118	0.9478	0.8774		
Wong2020Fast	0.5620	0.8467	0.7806		
Wu2020Adversarial	0.7150	0.9030	0.8691		
Wu2020Adversarial_extra	0.6646	0.9026	0.8182		
Xu2023Exploring_WRN-28-10	0.6841	0.9529	0.8869		
Zhang2019Theoretically	0.6505	0.8703	0.8070		
Zhang2019You	0.6472	0.8870	0.8586		
Zhang2020Attacks	0.6145	0.8682	0.8166		
Zhang2020Geometry	0.6526	0.9109	0.8316		

Table 10. All CIFAR-10 accuracy scores for the Noise distortion and the victim model ResNet-50.

Distortion	Victim Model	Dataset Model ID	Ours	CIFAR-10	CIFAR-10-C
Noise	VGG-16	Addepalli2021Towards_RN18	0.5032	0.7885	0.7383
		AGAT	0.2747	0.8396	0.6173
		Addepalli2021Towards_WRN34	0.4837	0.8314	0.7422
		Addepalli2022Efficient_RN18	0.5281	0.8398	0.7899
		Addepalli2022Efficient_WRN_34_10	0.5810	0.8739	0.8173
		Andriushchenko2020Understanding	0.4590	0.7731	0.7276
		Augustin2020Adversarial	0.4960	0.9076	0.7703
		Augustin2020Adversarial_34_10	0.5438	0.9230	0.8092
		Augustin2020Adversarial_34_10_extra	0.5480	0.9440	0.8688
		Carmon2019Unlabeled	0.5347	0.8917	0.8059
		Chen2020Adversarial	0.4795	0.8281	0.7701
		Chen2020Efficient	0.5126	0.8307	0.7740
		Chen2021LTD_WRN34_10	0.5246	0.8310	0.7734
		Chen2021LTD_WRN34_20	0.5074	0.8432	0.7796
		Cui2020Learnable_34_10	0.5380	0.8740	0.8084
		Cui2020Learnable_34_20	0.5197	0.8656	0.8083
		Dai2021Parameterizing	0.5525	0.8528	0.7875
		Debenedetti2022Light_XCIT-L12	0.5983	0.9046	0.8350
		Debenedetti2022Light_XCIT-M12	0.5891	0.9026	0.8249
		Debenedetti2022Light_XCIT-S12	0.5501	0.8851	0.8227
		Diffenderfer2021Winning_Binary	0.4162	0.9693	0.8220
		Diffenderfer2021Winning_Binary_CARD_Deck	0.5439	0.9727	0.9179
		Diffenderfer2021Winning_LRR	0.5013	0.9885	0.7997
		Diffenderfer2021Winning_LRR_CARD_Deck	0.6036	0.9868	0.9287
		Ding2020MMA	0.5709	0.8708	0.8160
		Engstrom2019Robustness	0.5803	0.9069	0.8481
		Gowal2020Uncovering	0.6615	0.9083	0.8722
		Gowal2020Uncovering_28_10_extra	0.5421	0.8935	0.8177
		Gowal2020Uncovering_34_20	0.5406	0.8415	0.7916
		Gowal2020Uncovering_70_16	0.5191	0.8392	0.7906
		Gowal2020Uncovering_70_16_extra	0.5618	0.9085	0.8253
		Gowal2020Uncovering_extra	0.5631	0.9566	0.8801
		Gowal2021Improving_28_10_ddpm_100m	0.5102	0.8656	0.7819
		Gowal2021Improving_70_16_ddpm_100m	0.5370	0.8720	0.7854
		Gowal2021Improving_R18_ddpm_100m	0.5306	0.8537	0.7999
		Hendrycks2019Using	0.4791	0.8598	0.7641
		Hendrycks2020AugMix_ResNeXt	0.4902	0.9714	0.7719
		Hendrycks2020AugMix_WRN	0.4321	0.9647	0.7947
		Huang2020Self	0.5097	0.8137	0.7677
		Huang2021Exploring	0.5617	0.9030	0.8124
		Huang2021Exploring_ema	0.5506	0.9125	0.8258
		Huang2022Revisiting_WRN-A4	0.5476	0.9163	0.8247
		Jia2022LAS-AT_34_10	0.5171	0.8264	0.7678
		Jia2022LAS-AT_70_16	0.5208	0.8388	0.7792
		Kang2021Stable	0.5015	0.9394	0.8511
		Kireev2021Effectiveness_AugMixNoJSD	0.3938	0.9711	0.7575
		Kireev2021Effectiveness_Gauss50percent	0.5638	0.9441	0.9199
		Kireev2021Effectiveness_RLAT	0.5114	0.9409	0.8565
		Kireev2021Effectiveness_RLATAugMix	0.4918	0.9635	0.8592
		Kireev2021Effectiveness_RLATAugMixNoJSD	0.4707	0.9735	0.8508
		Modas2021PRIMEResNet18	0.7093	0.9283	0.8717
		Pang2020Boosting	0.5028	0.8363	0.7551
		Pang2022Robustness_WRN28_10	0.5092	0.8691	0.8095
		Pang2022Robustness_WRN70_16	0.5106	0.8681	0.8062
		Rade2021Helper_R18_ddpm	0.6194	0.9110	0.8575
		Rade2021Helper_R18_extra	0.4385	0.8784	0.7991
		Rade2021Helper_ddpm	0.5347	0.8685	0.7604
		Rade2021Helper_extra	0.5613	0.9094	0.8311
		Rebuffi2021Fixing_106_16_cutmix_ddpm	0.5111	0.8719	0.7952
		Rebuffi2021Fixing_28_10_cutmix_ddpm	0.5463	0.9079	0.8515
Rebuffi2021Fixing_70_16_cutmix_ddpm	0.4920	0.8749	0.8001		
Rebuffi2021Fixing_70_16_cutmix_extra	0.5225	0.9605	0.8520		
Rebuffi2021Fixing_70_16_cutmix_extra_L2	0.5225	0.9605	0.8520		
Rebuffi2021Fixing_70_16_cutmix_extra_Linf	0.5047	0.9191	0.8190		
Rebuffi2021Fixing_R18_cutmix_ddpm	0.5580	0.8915	0.8251		
Rebuffi2021Fixing_R18_ddpm	0.5093	0.8133	0.7573		
Rice2020Overfitting	0.5758	0.8678	0.8173		
Rony2019Decoupling	0.5889	0.8985	0.8656		
Schwag2020Hydra	0.5441	0.8718	0.8104		
Schwag2021Proxy	0.5923	0.8937	0.8360		
Schwag2021Proxy_R18	0.5687	0.8839	0.8316		
Schwag2021Proxy_ResNest152	0.5531	0.8587	0.7847		
Sitawarin2020Improving	0.5113	0.8612	0.8043		
Sridhar2021Robust	0.5443	0.8887	0.7959		
Sridhar2021Robust_34_15	0.5247	0.8558	0.7708		
Standard	0.2984	0.9713	0.4432		
Wang2020Improving	0.5365	0.8621	0.7723		
Wang2023Better_WRN-28-10	0.5613	0.9187	0.8421		
Wang2023Better_WRN-70-16	0.5786	0.9603	0.8738		
Wong2020Fast	0.4447	0.8189	0.7458		
Wu2020Adversarial	0.6023	0.8640	0.8377		
Wu2020Adversarial_extra	0.5333	0.8746	0.7786		
Xu2023Exploring_WRN-28-10	0.5556	0.9329	0.8545		
Zhang2019Theoretically	0.5145	0.8328	0.7588		
Zhang2019You	0.5182	0.8453	0.8175		
Zhang2020Attacks	0.5097	0.8296	0.7793		
Zhang2020Geometry	0.5153	0.8828	0.7961		

Table 11. All CIFAR-10 accuracy scores for the Noise distortion and the victim model VGG-16.

References

- [1] Sara Beery, Elijah Cole, and Arvi Gjoka. The iwildcam 2020 competition dataset. *arXiv preprint arXiv:2004.10340*, 2020. [2](#)
- [2] Nicholas Carlini, Anish Athalye, Nicolas Papernot, Wieland Brendel, Jonas Rauber, Dimitris Tsipras, Ian Goodfellow, Aleksander Madry, and Alexey Kurakin. On evaluating adversarial robustness. *arXiv preprint arXiv:1902.06705*, 2019. [5](#), [9](#)
- [3] Jeremy Cohen, Elan Rosenfeld, and Zico Kolter. Certified adversarial robustness via randomized smoothing. In *international conference on machine learning*, pages 1310–1320. PMLR, 2019. [5](#), [9](#)
- [4] Francesco Croce, Maksym Andriushchenko, Vikash Sehwag, Edoardo DeBenedetti, Nicolas Flammarion, Mung Chiang, Prateek Mittal, and Matthias Hein. RobustBench: a standardized adversarial robustness benchmark. In *Thirty-fifth Conference on Neural Information Processing Systems Datasets and Benchmarks Track*, pages 1–17, 2021. [5](#), [6](#), [9](#), [12](#), [13](#)
- [5] Francesco Croce and Matthias Hein. Reliable evaluation of adversarial robustness with an ensemble of diverse parameter-free attacks. In *International conference on machine learning*, pages 2206–2216. PMLR, 2020. [2](#)
- [6] Ekin D Cubuk, Barret Zoph, Dandelion Mane, Vijay Vasudevan, and Quoc V Le. Autoaugment: Learning augmentation policies from data. *arXiv preprint arXiv:1805.09501*, 2018. [2](#)
- [7] Ekin D Cubuk, Barret Zoph, Jonathon Shlens, and Quoc V Le. Randaugment: Practical automated data augmentation with a reduced search space. In *Proceedings of the IEEE/CVF conference on computer vision and pattern recognition workshops*, pages 702–703, 2020. [2](#)
- [8] Jia Deng, Wei Dong, Richard Socher, Li-Jia Li, Kai Li, and Li Fei-Fei. Imagenet: A large-scale hierarchical image database. In *IEEE Conference on Computer Vision and Pattern Recognition*, pages 248–255. IEEE, 2009. [12](#)
- [9] Terrance DeVries and Graham W Taylor. Improved regularization of convolutional neural networks with cutout. *arXiv preprint arXiv:1708.04552*, 2017. [2](#)
- [10] James Diffenderfer, Brian R. Bartoldson, Shreya Chaganti, Jize Zhang, and Bhavya Kailkhura. A winning hand: Compressing deep networks can improve out-of-distribution robustness. In Marc’Aurelio Ranzato, Alina Beygelzimer, Yann N. Dauphin, Percy Liang, and Jennifer Wortman Vaughan, editors, *Advances in Neural Information Processing Systems 34: Annual Conference on Neural Information Processing Systems 2021, NeurIPS 2021, December 6-14, 2021, virtual*, pages 664–676, 2021. [2](#), [6](#)
- [11] N. Benjamin Erichson, Soon Hoe Lim, Francisco Utrera, Winnie Xu, Ziang Cao, and Michael W. Mahoney. Noisymix: Boosting robustness by combining data augmentations, stability training, and noise injections. *CoRR*, abs/2202.01263, 2022. [2](#), [7](#)
- [12] Robert Geirhos, Patricia Rubisch, Claudio Michaelis, Matthias Bethge, Felix A. Wichmann, and Wieland Brendel. Imagenet-trained cnns are biased towards texture; increasing shape bias improves accuracy and robustness. In *7th International Conference on Learning Representations, ICLR 2019, New Orleans, LA, USA, May 6-9, 2019*. OpenReview.net, 2019. [2](#), [7](#)
- [13] Tejas Gokhale, Rushil Anirudh, Bhavya Kailkhura, Jayaraman J Thiagarajan, Chitta Baral, and Yezhou Yang. Attribute-guided adversarial training for robustness to natural perturbations. In *Proceedings of the AAAI Conference on Artificial Intelligence*, volume 35, pages 7574–7582, 2021. [15](#)
- [14] Tejas Gokhale, Rushil Anirudh, Jayaraman J Thiagarajan, Bhavya Kailkhura, Chitta Baral, and Yezhou Yang. Improving diversity with adversarially learned transformations for domain generalization. In *Proceedings of the IEEE/CVF Winter Conference on Applications of Computer Vision*, pages 434–443, 2023. [2](#)
- [15] Kaiming He, Xiangyu Zhang, Shaoqing Ren, and Jian Sun. Deep residual learning for image recognition. In *Proceedings of the IEEE conference on computer vision and pattern recognition*, pages 770–778, 2016. [13](#)
- [16] Dan Hendrycks, Steven Basart, Norman Mu, Saurav Kadavath, Frank Wang, Evan Dorundo, Rahul Desai, Tyler Zhu, Samyak Parajuli, Mike Guo, Dawn Song, Jacob Steinhardt, and Justin Gilmer. The many faces of robustness: A critical analysis of out-of-distribution generalization. In *2021 IEEE/CVF International Conference on Computer Vision, ICCV 2021, Montreal, QC, Canada, October 10-17, 2021*, pages 8320–8329. IEEE, 2021. [7](#)
- [17] Dan Hendrycks and Thomas G. Dietterich. Benchmarking neural network robustness to common corruptions and perturbations. In *7th International Conference on Learning Representations, ICLR 2019, New Orleans, LA, USA, May 6-9, 2019*. OpenReview.net, 2019. [1](#), [2](#), [6](#), [12](#)
- [18] Dan Hendrycks, Norman Mu, Ekin Dogus Cubuk, Barret Zoph, Justin Gilmer, and Balaji Lakshminarayanan. Augmix: A simple data processing method to improve robustness and uncertainty. In *8th International Conference on Learning Representations, ICLR 2020, Addis Ababa, Ethiopia, April 26-30, 2020*. OpenReview.net, 2020. [2](#), [6](#), [7](#)
- [19] J. D. Hunter. Matplotlib: A 2d graphics environment. *Computing in Science & Engineering*, 9(3):90–95, 2007. [13](#)
- [20] Klim Kireev, Maksym Andriushchenko, and Nicolas Flammarion. On the effectiveness of adversarial training against common corruptions. In James Cussens and Kun Zhang, editors, *Uncertainty in Artificial Intelligence, Proceedings of the Thirty-Eighth Conference on Uncertainty in Artificial Intelligence, UAI 2022, 1-5 August 2022, Eindhoven, The Netherlands*, volume 180 of *Proceedings of Machine Learning Research*, pages 1012–1021. PMLR, 2022. [2](#), [6](#)
- [21] Thomas Kluyver, Benjamin Ragan-Kelley, Fernando Pe’rez, Brian Granger, Matthias Bussonnier, Jonathan Frederic, Kyle Kelley, Jessica Hamrick, Jason Grout, Sylvain Corlay, Paul Ivanov, Damia’n Avila, Safia Abdalla, Carol Willing, and Jupyter development team. Jupyter notebooks - a publishing format for reproducible computational workflows. In Fernando Loizides and Birgit Schmidt, editors, *Positioning and Power in Academic Publishing: Players, Agents and Agendas*, pages 87–90, Netherlands, 2016. IOS Press. [13](#)

- [22] Alex Krizhevsky. Learning multiple layers of features from tiny images. Technical report, University of Toronto, 2009. [12](#)
- [23] Alex Krizhevsky, Geoffrey Hinton, et al. Learning multiple layers of features from tiny images. 2009. [6](#)
- [24] Da Li, Yongxin Yang, Yi-Zhe Song, and Timothy M Hospedales. Deeper, broader and artier domain generalization. In *Proceedings of the IEEE international conference on computer vision*, pages 5542–5550, 2017. [2](#)
- [25] Apostolos Modas, Rahul Rade, Guillermo Ortiz-Jime'nez, Seyed-Mohsen Moosavi-Dezfooli, and Pascal Frossard. PRIME: A few primitives can boost robustness to common corruptions. In Shai Avidan, Gabriel J. Brostow, Moustapha Cisse', Giovanni Maria Farinella, and Tal Hassner, editors, *Computer Vision - ECCV 2022 - 17th European Conference, Tel Aviv, Israel, October 23-27, 2022, Proceedings, Part XXV*, volume 13685 of *Lecture Notes in Computer Science*, pages 623–640. Springer, 2022. [2](#), [6](#)
- [26] Sajad Mousavi, Ricardo Luna Gutie'rrez, Desik Rengaranjan, Vineet Gundecha, Ashwin Ramesh Babu, Avisek Naug, Antonio Guillen, and Soumyendu Sarkar. N-critics: Self-refinement of large language models with ensemble of critics, 2023. [2](#)
- [27] Norman Mu and Justin Gilmer. Mnist-c: A robustness benchmark for computer vision. *arXiv preprint arXiv:1906.02337*, 2019. [2](#)
- [28] Arvind Neelakantan, Luke Vilnis, Quoc V Le, Ilya Sutskever, Lukasz Kaiser, Karol Kurach, and James Martens. Adding gradient noise improves learning for very deep networks. *arXiv preprint arXiv:1511.06807*, 2015. [9](#)
- [29] The pandas development team. pandas-dev/pandas: Pandas, Feb. 2020. [13](#)
- [30] Adam Paszke, Sam Gross, Francisco Massa, Adam Lerer, James Bradbury, Gregory Chanan, Trevor Killeen, Zeming Lin, Natalia Gimelshein, Luca Antiga, Alban Desmaison, Andreas Kopf, Edward Yang, Zachary DeVito, Martin Raison, Alykhan Tejani, Sasank Chilamkurthy, Benoit Steiner, Lu Fang, Junjie Bai, and Soumith Chintala. PyTorch: An Imperative Style, High-Performance Deep Learning Library. In H. Wallach, H. Larochelle, A. Beygelzimer, F. d'Alche' Buc, E. Fox, and R. Garnett, editors, *Advances in Neural Information Processing Systems 32*, pages 8024–8035. Curran Associates, Inc., 2019. [13](#)
- [31] Ben Poole, Jascha Sohl-Dickstein, and Surya Ganguli. Analyzing noise in autoencoders and deep networks. *arXiv preprint arXiv:1406.1831*, 2014. [9](#)
- [32] Raghavendran Ramakrishnan, Bhadrinath Nagabandi, Jose Eusebio, Shayok Chakraborty, Hemanth Venkateswara, and Sethuraman Panchanathan. Deep hashing network for unsupervised domain adaptation. In *Domain Adaptation in Computer Vision with Deep Learning*, pages 57–74. Springer, 2020. [2](#)
- [33] Soumyendu Sarkar, Ashwin Ramesh Babu, Vineet Gundecha, Antonio Guillen, Sajad Mousavi, Ricardo Luna, Sahand Ghorbanpour, and Avisek Naug. Rl-cam: Visual explanations for convolutional networks using reinforcement learning. In *Proceedings of the IEEE/CVF Conference on Computer Vision and Pattern Recognition*, pages 3860–3868, 2023. [2](#)
- [34] Soumyendu Sarkar, Ashwin Ramesh Babu, Vineet Gundecha, Antonio Guillen, Sajad Mousavi, Ricardo Luna, Sahand Ghorbanpour, and Avisek Naug. Robustness with query-efficient adversarial attack using reinforcement learning. In *Proceedings of the IEEE/CVF Conference on Computer Vision and Pattern Recognition*, pages 2329–2336, 2023. [2](#)
- [35] Soumyendu Sarkar, Ashwin Ramesh Babu, Sajad Mousavi, Sahand Ghorbanpour, Vineet Gundecha, Ricardo Luna Gutierrez, Antonio Guillen, and Avisek Naug. Reinforcement learning based black-box adversarial attack for robustness improvement. In *2023 IEEE 19th International Conference on Automation Science and Engineering (CASE)*, pages 1–8. IEEE, 2023. [2](#)
- [36] Soumyendu Sarkar, Ashwin Ramesh Babu, Sajad Mousavi, Vineet Gundecha, Sahand Ghorbanpour, Alexander Shmakov, Ricardo Luna Gutierrez, Antonio Guillen, and Avisek Naug. Robustness with black-box adversarial attack using reinforcement learning. In *AAAI 2023: Proceedings of the Workshop on Artificial Intelligence Safety 2023 (SafeAI 2023)*, volume 3381. <https://ceur-ws.org/Vol-3381/8.pdf>, 2023. [2](#)
- [37] Soumyendu Sarkar, Vineet Gundecha, Sahand Ghorbanpour, Alexander Shmakov, Ashwin Ramesh Babu, Alexandre Pichard, and Mathieu Cocho. Skip training for multi-agent reinforcement learning controller for industrial wave energy converters. In *2022 IEEE 18th International Conference on Automation Science and Engineering (CASE)*, pages 212–219. IEEE, 2022. [2](#)
- [38] Soumyendu Sarkar, Vineet Gundecha, Sahand Ghorbanpour, Alexander Shmakov, Ashwin Ramesh Babu, Avisek Naug, Alexandre Pichard, and Mathieu Cocho. Function approximation for reinforcement learning controller for energy from spread waves. In Edith Elkind, editor, *Proceedings of the Thirty-Second International Joint Conference on Artificial Intelligence, IJCAI-23*, pages 6201–6209. International Joint Conferences on Artificial Intelligence Organization, 8 2023. AI for Good. [2](#)
- [39] Soumyendu Sarkar, Vineet Gundecha, Alexander Shmakov, Sahand Ghorbanpour, Ashwin Ramesh Babu, Paolo Faraboschi, Mathieu Cocho, Alexandre Pichard, and Jonathan Fievez. Multi-objective reinforcement learning controller for multi-generator industrial wave energy converter. In *NeurIPS Tackling Climate Change with Machine Learning Workshop*, 2021. [2](#)
- [40] Soumyendu Sarkar, Vineet Gundecha, Alexander Shmakov, Sahand Ghorbanpour, Ashwin Ramesh Babu, Paolo Faraboschi, Mathieu Cocho, Alexandre Pichard, and Jonathan Fievez. Multi-agent reinforcement learning controller to maximize energy efficiency for multi-generator industrial wave energy converter. In *Proceedings of the AAAI Conference on Artificial Intelligence*, volume 36, pages 12135–12144, 2022. [2](#)
- [41] Soumyendu Sarkar, Sajad Mousavi, Ashwin Ramesh Babu, Vineet Gundecha, Sahand Ghorbanpour, and Alexander K Shmakov. Measuring robustness with black-box adversarial

- attack using reinforcement learning. In *NeurIPS ML Safety Workshop*, 2022. 2
- [42] Soumyendu Sarkar, Avisek Naug, Antonio Guillen, Ricardo Luna Gutierrez, Sahand Ghorbanpour, Sajad Mousavi, Ashwin Ramesh Babu, and Vineet Gundecha. Concurrent carbon footprint reduction (c2fr) reinforcement learning approach for sustainable data center digital twin. In *2023 IEEE 19th International Conference on Automation Science and Engineering (CASE)*, pages 1–8, 2023. 2
- [43] Jiri Sedlar, Karla Stepanova, Radoslav Skoviera, Jan K Behrens, Matus Tuna, Gabriela Sejnova, Josef Sivic, and Robert Babuska. Imitrob: Imitation learning dataset for training and evaluating 6d object pose estimators. *IEEE Robotics and Automation Letters*, 8(5):2788–2795, 2023. 2
- [44] Alexander Shmakov, Avisek Naug, Vineet Gundecha, Sahand Ghorbanpour, Ricardo Luna Gutierrez, Ashwin Ramesh Babu, Antonio Guillen, and Soumyendu Sarkar. Rtdk-bo: High dimensional bayesian optimization with reinforced transformer deep kernels. In *2023 IEEE 19th International Conference on Automation Science and Engineering (CASE)*, pages 1–8. IEEE, 2023. 2
- [45] Karen Simonyan and Andrew Zisserman. Very deep convolutional networks for large-scale image recognition. *arXiv preprint arXiv:1409.1556*, 2014. 13
- [46] Christian Szegedy, Wei Liu, Yangqing Jia, Pierre Sermanet, Scott Reed, Dragomir Anguelov, Dumitru Erhan, Vincent Vanhoucke, and Andrew Rabinovich. Going deeper with convolutions. In *Proceedings of the IEEE conference on computer vision and pattern recognition*, pages 1–9, 2015. 13
- [47] Rui Tian, Zuxuan Wu, Qi Dai, Han Hu, and Yugang Jiang. Deeper insights into vits robustness towards common corruptions. *arXiv preprint arXiv:2204.12143*, 2022. 2, 7
- [48] Guido Van Rossum and Fred L Drake Jr. *Python reference manual*. Centrum voor Wiskunde en Informatica Amsterdam, 1995. 13
- [49] Vikas Verma, Alex Lamb, Christopher Beckham, Amir Najafi, Ioannis Mitliagkas, David Lopez-Paz, and Yoshua Bengio. Manifold mixup: Better representations by interpolating hidden states. In *International conference on machine learning*, pages 6438–6447. PMLR, 2019. 2
- [50] Zekai Wang, Tianyu Pang, Chao Du, Min Lin, Weiwei Liu, and Shuicheng Yan. Better diffusion models further improve adversarial training. *CoRR*, abs/2302.04638, 2023. 2, 6
- [51] Michael Lawrence Waskom. seaborn: statistical data visualization. *Journal of Open Source Software*, 60, April 2021. 13
- [52] Zhenlin Xu, Deyi Liu, Junlin Yang, Colin Raffel, and Marc Niethammer. Robust and generalizable visual representation learning via random convolutions. *arXiv preprint arXiv:2007.13003*, 2020. 2
- [53] Sangdoon Yun, Dongyoon Han, Seong Joon Oh, Sanghyuk Chun, Junsuk Choe, and Youngjoon Yoo. Cutmix: Regularization strategy to train strong classifiers with localizable features. In *Proceedings of the IEEE/CVF international conference on computer vision*, pages 6023–6032, 2019. 2
- [54] Hongyi Zhang, Moustapha Cisse', Yann N. Dauphin, and David Lopez-Paz. mixup: Beyond empirical risk minimization. In *6th International Conference on Learning Representations, ICLR 2018, Vancouver, BC, Canada, April 30 - May 3, 2018, Conference Track Proceedings*. OpenReview.net, 2018. 2